



Article

The Use of Biomass-Derived Chitosan for Colorimetric pH Detection

Ezekiel Edward Nettey-Oppong ^{1,†}, Riaz Muhammad ^{1,†}, Dohyun Yoo ^{1,†}, Sun-Hyeop Hwang ^{1,†}, Ahmed Ali ^{1,2,*}, Chacha Saidi Mwita ¹, Hyun-Woo Jeong ³, Seong-Wan Kim ⁴, Young-Seek Seok ^{5,*} and Seung Ho Choi ^{1,6,*}

- Department of Biomedical Engineering, Yonsei University, Wonju 26493, Republic of Korea; ezekieledward@yonsei.ac.kr (E.E.N.-O.); riaz@yonsei.ac.kr (R.M.); yoodohyun@yonsei.ac.kr (D.Y.); creamer9837@yonsei.ac.kr (S.-H.H.); chachasaidimwita@yonsei.ac.kr (C.S.M.)
- ² Department of Electrical Engineering, Sukkur IBA University, Sukkur 65200, Pakistan
- Department of Biomedical Engineering, Eulji University, Seongnam 13135, Republic of Korea; hwjeong@eulji.ac.kr
- Department of Agricultural Biology, National Institute of Agricultural Sciences, Rural Development Administration, Wanju 55365, Republic of Korea; tarupa@korea.kr
- Gangwon-do Agricultural Product Registered Seed Station, Chuncheon 24410, Republic of Korea
- Department of Integrative Medicine, Major in Digital Healthcare, Yonsei University College of Medicine, Seoul 06229, Republic of Korea
- * Correspondence: alee@yonsei.ac.kr (A.A.); air5738@korea.kr (Y.-S.S.); seunghochoi@yonsei.ac.kr (S.H.C.); Tel.: +82-33-760-2463 (S.H.C.)
- [†] These authors contributed equally to this work.

Abstract: This study developed a sustainable colorimetric pH sensor using chitosan derived from mealworm (Tenebrio molitor) biomass and anthocyanin extracted from red cabbage (Brassica oleracea). Chitosan was used as the substrate material, and anthocyanin served as the pH indicator dye, collectively forming the basis of the pH sensor. The resulting pHresponsive film effectively measures pH levels from 1 to 13, with a distinct color shift from pink to green. The sensor demonstrated remarkable stability, maintaining color fidelity after prolonged exposure to aqueous environments, and its practical functionality was confirmed through an ammonia detection assay, underscoring its utility in monitoring food freshness. Mechanistic investigations using Fourier-transform infrared spectroscopy (FTIR) and molecular modeling identified electrostatic and hydrophobic forces as key factors in anthocyanin binding to the chitosan matrix. Molecular modeling further revealed a minimal binding energy of -3 kcal/mol and an RMSD of 0 Å, indicating a strong interaction stability. The film exhibited high structural integrity, with tensile strength and elongation values of 8.8 MPa and 8.4%, respectively, and its flexibility suggests its suitability for diverse applications, including biomedical devices. The eco-friendly production process and the biocompatibility of this sensor provide a sustainable alternative to conventional pH measurement technologies. This innovation not only addresses ecological challenges but also expands the capabilities of colorimetric sensors for use in scientific research, biomedical applications, and other fields.

Keywords: colorimetric pH sensor; anthocyanin; chitosan; biomass; molecular modeling



Received: 8 January 2025 Revised: 17 February 2025 Accepted: 18 February 2025 Published: 4 March 2025

Citation: Nettey-Oppong, E.E.; Muhammad, R.; Yoo, D.; Hwang, S.-H.; Ali, A.; Mwita, C.S.; Jeong, H.-W.; Kim, S.-W.; Seok, Y.-S.; Choi, S.H. The Use of Biomass-Derived Chitosan for Colorimetric pH Detection. *Photonics* 2025, 12, 231. https://doi.org/10.3390/ photonics12030231

Copyright: © 2025 by the authors. Licensee MDPI, Basel, Switzerland. This article is an open access article distributed under the terms and conditions of the Creative Commons Attribution (CC BY) license (https://creativecommons.org/licenses/by/4.0/).

1. Introduction

Diverse substrates have been integrated with a variety of sensing techniques, such as colorimetric, electroluminescent, electrochemical, and ion detection methods, to create high-performance sensors [1–5]. These sensors offer non-invasive, real-time monitoring and

Photonics **2025**, 12, 231 2 of 34

continuous detection capabilities. Essential to the effectiveness and widespread application of sensors are the biocompatibility and flexibility of their substrate. This has prompted the utilization of a range of materials, such as textiles [6], tattoos [7], paper [8], and stretchable elastomers [9]. Among the sensing techniques, colorimetry holds distinct advantages due to its simplicity, cost-effectiveness, and the ease with which signals can be observed and interpreted by the unaided eye. Naked-eye-readable colorimetric sensors find value across diverse applications, including clinical usage, environmental monitoring, and agri-food technologies [10–12]. The measurement of pH serves as a critical parameter reflecting various chemical conditions pertinent to biological functions and chemical processes in fields ranging from biochemistry and environmental science to general chemistry [13–15]. While electrochemical pH meters with glass electrodes dominate the commercial market owing to their accuracy and affordability, optical pH sensors have garnered substantial attention due to their unique advantages over conventional pH electrodes. These advantages include lower costs, absence of electrical contacts, high levels of miniaturization, elimination of the need for frequent calibration, and suitability for safe in-vivo measurements [16,17].

Conventionally, pH-sensitive dyes have been used to create optical pH sensors by their immobilization on a substrate. Promphet et al. [18] developed a colorimetric sensor based on textiles capable of concurrently detecting the pH of sweat and lactate levels. This was accomplished by sequentially depositing three distinct layers, namely sodium carboxymethyl cellulose, chitosan, and a pH dye or an assay for lactate onto a cotton fabric substrate. Similarly, Ha et al. [6] introduced a wearable pH sensor utilizing a smart textile constructed from curcumin thermoplastic polyurethane, primarily designed for health diagnostics through the analysis of sweat pH levels. Furthermore, Yapor et al. [19] employed polydiacetylene nanofiber composites, a combination of 10,12-pentacosadiynoic acid and a supporting polymer containing poly(ethylene oxide) and polyurethane, to create a colorimetric sensor capable of detecting Escherichia coli and variations in pH values. Finnegan et al. [20] devised a wearable colorimetric sensor based on bromocresol green to identify volatile emissions from the skin surface, facilitating the precise monitoring of skin pH levels. However, it is worth noting that these conventional pH sensors frequently rely on pristine substrate materials and synthetic dye indicators, often overlooking a more sustainable approach. This prevailing practice has spurred the investigation of alternative methods to overcome limitations for improvement and innovation in colorimetric pH sensor design and fabrication. The ever-increasing demand for sustainable technologies necessitates the exploration of alternative sources of materials for substrates and indicator dyes for pH sensor development.

Mealworms stand out among insect species for their suitability for large scale production, easily adaptable biological requirements, and extensive existing knowledge base that allows commercial insect producers to effectively meet current market demands [21]. However, the proliferation of mealworm commercialization has led to a consequential increase in biomass waste generation during the rearing process, causing environmental concerns. This generated waste emerges as a prospective raw material for the extraction of chitosan. Chitosan is an exceptionally versatile biopolymer [22]. Notably, owing to its inherent degradability, biocompatibility, and lack of cytotoxicity, chitosan has been extensively employed in diverse applications, including water treatment [23,24], drug delivery [25], tissue engineering [26], and cosmetics [27]. Additionally, the unique structural and surface properties of chitosan offer opportunities for tailored degradation, proving advantageous for its use [28].

Anthocyanins are a class of glycosylated polyhydroxy and polymethoxy derivatives of 2-phenylbenzopyrylium salts, which are pivotal in conferring the vibrant hues observed in numerous fruits, vegetables, and flowers [29,30]. Within this category, red cabbage (*Brassica*

Photonics **2025**, 12, 231 3 of 34

oleracea L.) emerges as a particularly notable source of anthocyanins. Distinguished by their exceptional characteristic, the anthocyanins derived from red cabbage possess the unique ability to manifest coloration across a wide pH range. This contrasts with anthocyanins sourced from alternate origins, such as black currant, grape skin, and elderberry, which exhibit significant coloration primarily at pH levels below 4 [31]. Notably, the chromatic range of anthocyanins derived from red cabbage encompasses shades ranging from red in acidic environments to green in alkaline conditions [32]. Consequently, their utility is not confined solely to acidic pH changes.

Through the utilization of chitosan extracted from biomass waste and anthocyanin from red cabbage, an economically viable and ecologically sustainable approach to pH sensing can be realized. The combination of readily available raw materials and a simple fabrication process renders the mass production of chitosan-based pH sensors both feasible and capable of maintaining high-performance levels. This study introduces a biomass-derived pH sensor film developed from chitosan sourced from mealworm shells and anthocyanin extracted from red cabbage. Through FTIR characterization and a comprehensive analysis of the physicochemical and mechanical properties, we confirmed the structural integrity and suitability of the fabricated film for pH-sensing applications. Molecular modeling provides insights into the interactions between anthocyanins and chitosan. Additionally, durability and color stability were confirmed over time, and the flexibility of the chitosan substrate facilitated easy folding, thereby enhancing its versatility for various applications. Further sensitivity quantification through an ammonia assay demonstrated the capability of the sensor to monitor pH in real time.

2. Materials and Methods

2.1. Materials

The mealworm shells provided by the Rural Development Administration of the Republic of Korea were the primary materials in this study. Red cabbage was obtained from a local supermarket. Sodium Hydroxide (NaOH) with >98.0% purity and 40.00 g/mol molecular weight was procured from OCI-company Ltd., Seoul, Republic of Korea. Acetic Acid (CH₃COOH) was obtained from DAEJUNG Reagents Chemicals & Metals Co., Ltd., Siheung, Republic of Korea, with >99.5% purity and 60.05 g/mol molecular weight. In addition, 28% ammonia solution was acquired from JUNSEI Chemical Co., Ltd., Tokyo, Japan. Additionally, pH buffer solutions obtained from Dongsung Corporation Co., Ltd., Seoul, Republic of Korea, and miracloth 475855-1R filter paper procured from EMD Millipore Corp, Burlington, MA, USA, were utilized in the experimental procedures.

Source of Biomass

The Gangwon Provincial Agricultural Products Center in Chuncheon, Republic of Korea, houses a smart factory that produces yellow mealworm beetles (*Tenebrio molitor*) on a large scale. The factory maintains the mealworms' ideal growth and health by regularly checking and modifying the environment through cutting-edge technologies employing artificial intelligence and the Internet of Things. The breeding strategy focuses on high fecundity, rapid development, and high survivability, which are supported by rigorous genetic evaluation and species selection criteria. Through this innovative smart farming approach, the smart factory produces 10 tons of mealworms annually. The high production rate of mealworms generates a significant amount of biomass from which chitosan can be extracted.

Photonics **2025**, 12, 231 4 of 34

2.2. Extraction of Chitosan

The procedure for extracting chitosan from mealworm shells involves a systematic series of steps. Initially, biomass waste derived from mealworms, specifically mealworm shells, was collected and served as the primary raw material. The collected waste underwent an initial pretreatment stage involving manual cleaning to eliminate any residual traces of worms or other impurities. Subsequently, the mealworm shells were subjected to a meticulous cleaning process using hot water to eradicate dirt particles and undesired substances. The sample was then dried in a ventilated oven, resulting in the formation of dry mealworm shell flakes. These flakes were subsequently finely ground to obtain a powdered form and securely stored in a sealed container for subsequent use, which constituted the principal material for chitosan extraction.

The extraction process encompasses distinct phases, each contributing to the isolation and purification of chitosan from the mealworm shell flakes. Demineralization commenced with the dissolution of 5 g of the extracted powder in a 1 N acetic acid solution. The dissolution process spanned 12 h at 60 °C with constant agitation at 400 rpm. During the demineralization process, incremental addition of acid was conducted to mitigate potential foaming, a phenomenon induced by gas generation resulting from the existing calcium carbonate in the mealworm shells, which is a chemical reaction that produces carbon dioxide. Demineralization eliminates the mineral constituents of biomass, producing the organic matrix of interest.

Following demineralization, the sample underwent thorough rinsing with deionized water using a miracloth filter and was subsequently subjected to a drying period of 48 h at a temperature of 60 °C. After demineralization, the subsequent phase involved deproteinization, which was achieved through an alkali digestion process. This process effectively removed the inherent proteins linked with the chitin structure. The demineralized sample was immersed in a $2\% \ w/v$ sodium hydroxide solution for 12 h at 60 °C, with continuous stirring at 400 rpm. This step required thorough rinsing and subsequent drying, following the previously outlined procedure. The deproteinization phase led to the isolation of chitin in a more refined state, enabling the subsequent formation of chitosan.

The pivotal conversion of chitin to chitosan was achieved through a deacetylation process. The resulting chitin was treated with a concentrated alkali solution, specifically a 50%~w/v sodium hydroxide solution. The deacetylation process was conducted over a span of 5 days and under a temperature of $120~{\rm ^{\circ}C}$. Deacetylation results in the transformation of N-acetyl groups within the chitin structure into amino (NH₂) groups, culminating in the production of chitosan. This conversion enhances the solubility and adaptability of the material, rendering it suitable for a wide array of applications. The resulting chitosan was subsequently filtered and subjected to a thorough wash with deionized water to ensure its purity. The chitosan extraction process followed protocols previously established in the literature [33–35]. The visual representation in Figure 1 offers a clear illustration of each stage of the extraction process, providing a comprehensive overview of the conversion of biomass waste into chitosan. Additionally, it presents graphic representations of intermediary phases, showcasing the progressive development of the material.

2.3. Fabrication of the Chitosan-Based pH Sensor

The production of the chitosan-based pH sensor commenced with the extraction of anthocyanin from red cabbage, as illustrated in Figure 2a, followed by mixing the extracted chitosan and anthocyanin solutions and casting, as demonstrated in Figure 2b. The red cabbage leaves were first cut into small pieces. Thereafter, 25 g of the cut leaves were immersed in 50 mL of water for 2 h at a controlled temperature of 60 °C with continuous agitation at 400 rpm. The resulting anthocyanin extract was filtered through a miracloth to

Photonics **2025**, 12, 231 5 of 34

separate the leaves and remove any large particles. The resulting filtrate was subjected to centrifugation for 15 min at 6000 rpm to facilitate the removal of fine suspended particles in a separate step. The ratio of anthocyanin to chitosan used in the sensor fabrication was optimized to ensure structural integrity while maintaining adequate interaction with anthocyanin. Subsequently, 1 mL of 1.4 mg/mL extracted anthocyanin was added to 10 mL of 4% chitosan solution, cast onto a Petri dish, and allowed to dry for 48 h in a fume hood, yielding a final film with a total anthocyanin content of 14 mg. This process led to the incorporation of the anthocyanin—serving as the pH indicator dye—into the biomass-derived chitosan polymer matrix, constituting the chitosan-based pH sensor.

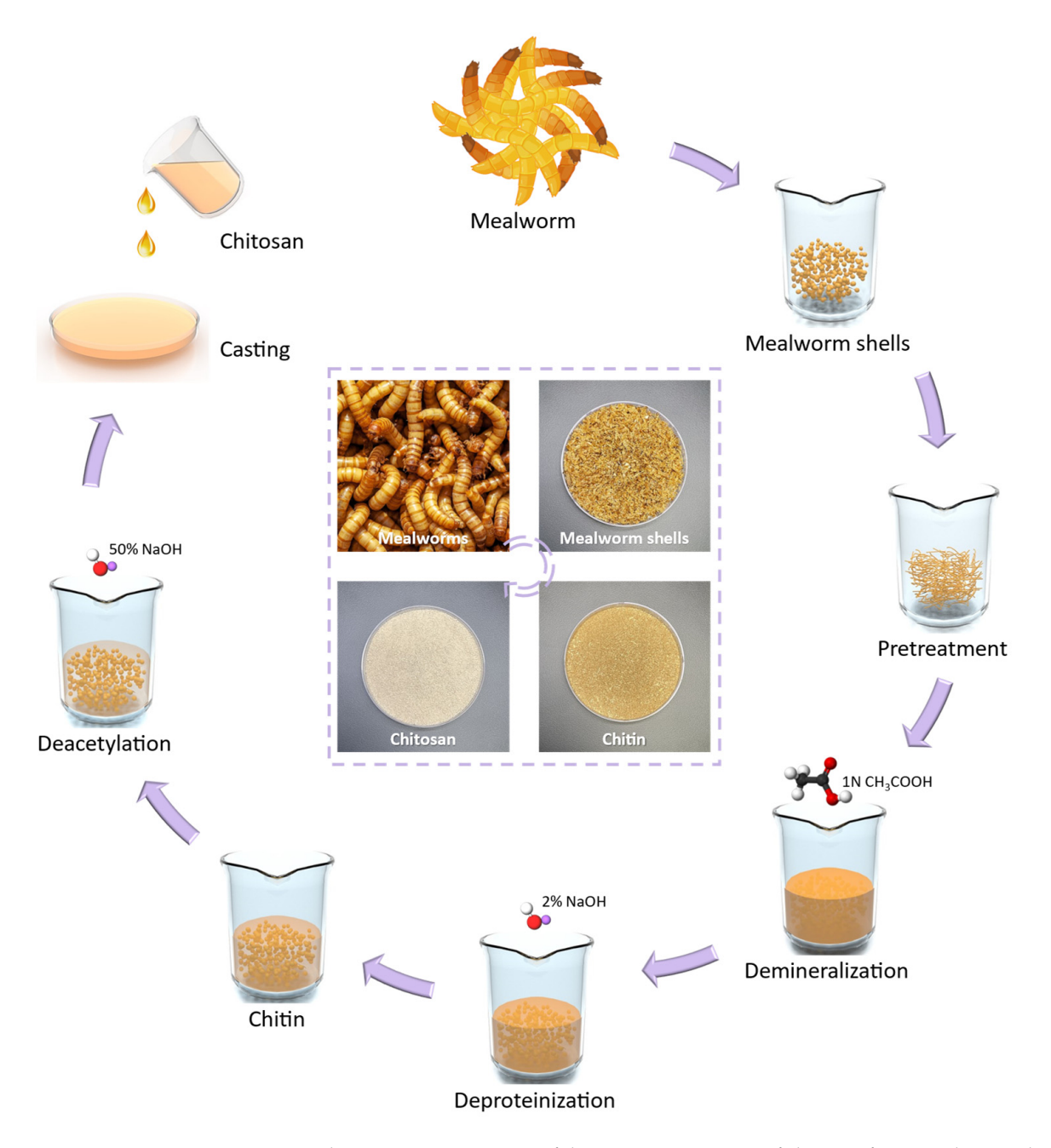
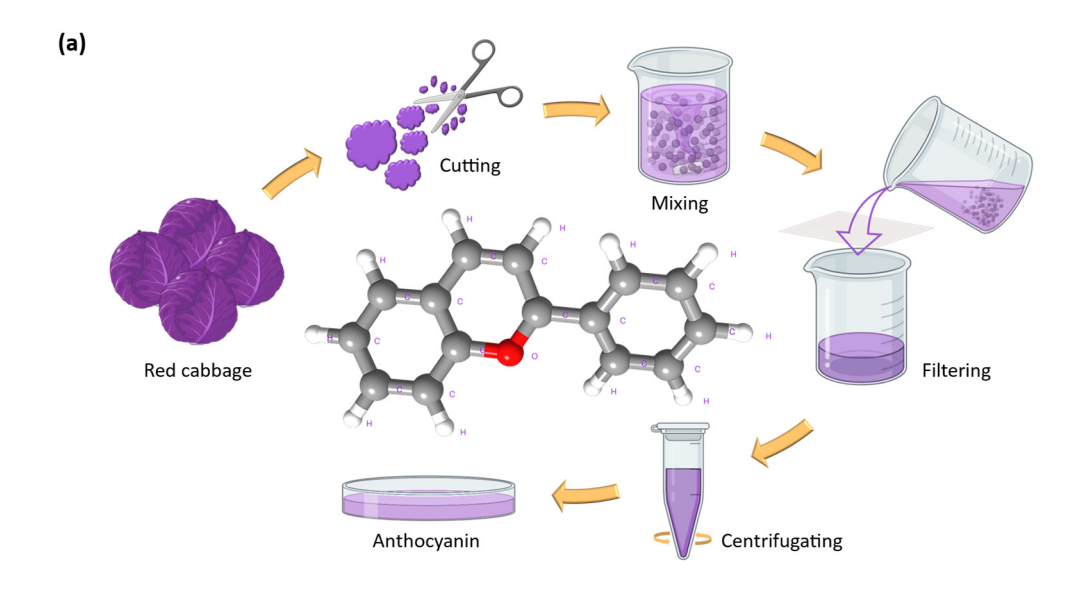


Figure 1. Schematic representation of the extraction process of chitosan from mealworm shells. The process involves pretreatment, demineralization with acetic acid, deproteinization with sodium hydroxide, and deacetylation to convert chitin into chitosan. Digital images at the center illustrate the key stages of extraction.

Photonics **2025**, 12, 231 6 of 34



(b)

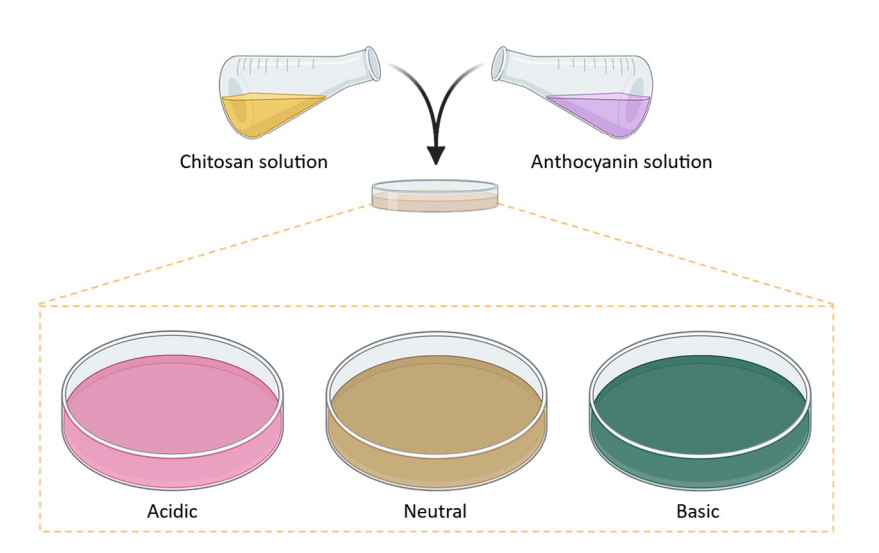


Figure 2. Schematic representation of the extraction of anthocyanin and fabrication of the chitosan-based pH sensor. (a) Stepwise process for extracting anthocyanin from red cabbage. The fresh leaves of the red cabbage are cut into small pieces and mixed with water for a specified period. Subsequently, the resulting extract undergoes filtration, followed by centrifugation. The central portion of the figure presents the chemical structure of anthocyanin, with each constituent element of the structure appropriately labeled. (b) pH sensor fabrication via casting. The as-synthesized chitosan solution was mixed with the anthocyanin solution and cast onto a Petri dish, resulting in the formation of a chitosan-based pH sensor. The fabricated sensor displays a discernible color transition from pink to green, corresponding to acidic and basic conditions, respectively.

The anthocyanin extract was not dried before incorporation; instead, it was directly mixed in solution form to preserve its halochromic properties and prevent degradation. The ratio of anthocyanin to chitosan was determined through iterative experimentation, balancing the need for sufficient pigment concentration to ensure clear color transitions while avoiding excessive hydrophilicity, which could compromise the film stability. To determine the optimal concentration, we evaluated a range of anthocyanin concentrations from 0.5 mg mL^{-1} to 3.0 mg mL^{-1} . The best balance between achieving a pronounced colorimetric response and preserving the structural integrity of the film without leaching

Photonics **2025**, 12, 231 7 of 34

was achieved through a durability assessment (see Section 2.10). An optimal concentration of 1.40 mg mL⁻¹ was identified to achieve the best performance, as excessive anthocyanin incorporation led to reduced structural integrity, while lower concentrations resulted in less distinguishable color shifts. This optimization process was critical for ensuring the reproducibility and functional efficiency of the sensor. Figure 2a provides a detailed visualization of the composition of anthocyanin at the molecular level. Anthocyanin extracted from red cabbage is predominantly composed of derivatives of cyanidin-3-diglucoside-5-glucoside. The pigment features aromatic acid acyl groups, primarily comprising ferulic, P-coumaric, and sinapic acids. Owing to its chemical structure, this pigment exhibits noteworthy characteristics, including thermal and photostability, considerable antioxidant capacity, and a wide ranging spectrum of colors [36]. As illustrated in Figure 2b, the resulting pH sensor exhibits an observable transition in color, appearing pink in highly acidic environments, brown under neutral conditions encompassing slightly acidic and basic pH levels, and green in strongly basic conditions.

2.4. Determination of Colorimetric Properties

The obtained pH buffer solutions, spanning a pH range from 1 to 13, were employed in the preparation of standard pH calibration charts. The anthocyanin solution was first evaluated by adding buffer solutions of varying pH levels to assess the changes in color and evaluate the effectiveness of the extracted dye, which is sensitive to pH changes. Furthermore, the fabricated chitosan-based pH sensor was assessed to determine its efficiency and durability in detecting pH variations. Buffer solutions were applied to the fabricated pH sensor films, and the subsequent color changes were characterized. The resulting alterations in color were represented within the International Commission on Illumination (CIE) color space, specifically the CIE-LAB and the CIE XYZ color spaces. In addition, the color-fastness of the chitosan-based pH sensor was evaluated by immersing the film in deionized water for 90 min. The surrounding water was observed over time. The pH-dependent color variations of the sensor were analyzed using an image-processing approach to ensure accuracy and reproducibility. Sensor images were captured using a 12 MP wide camera (f/1.8 aperture) under uniform lighting conditions to minimize the variations due to external illumination. The acquired images were subsequently processed using MATLAB (Version R2024a, MathWorks, Natick, MA, USA), where the RGB values were extracted and converted into a CIE-Lab color space for quantitative assessment. A pH calibration chart was constructed by correlating the recorded colorimetric responses with known pH values, enabling precise interpretation of the sensor output. This methodological approach ensured that the sensor provided consistent and quantifiable colorimetric changes across the entire pH range tested.

2.5. Ammonia Assay and Sensitivity Analysis

To assess the sensitivity of the chitosan-based pH sensor, the produced films, measuring 2×2 cm², were secured to the top area of a beaker with a capacity of 25 mL, which contained 10 mL of the ammonia solution. The exposure lasted for 30 min in a fume hood at room temperature (25 °C). The sensitivity to the color of the film was quantified using the following equation:

$$S = \frac{(r_i - r_f) + (g_i - g_f) + (b_i - b_f)}{r_i + g_i + b_i} \times 100$$
 (1)

where r_i , g_i , and b_i denote the red, green, and blue values before exposure, and r_f , g_f , and b_f represent the corresponding values after exposure to the ammonia solution.

Photonics **2025**, 12, 231 8 of 34

2.6. FTIR Characterization

The chemical structures of the biomass-extracted chitosan film, red cabbage-extracted anthocyanin, and fabricated chitosan-based pH sensor were assessed using a Fourier-transform infrared spectrometer (Alpha II, Bruker, Bremen, Germany). The distinctive spectral patterns of the prepared samples were analyzed to verify their chemical compositions.

2.7. Molecular Modeling of Chitosan and Anthocyanin

The structure of the fabricated chitosan-based pH sensor was further probed through molecular modeling to elucidate the interaction dynamics between chitosan and anthocyanin. A systematic molecular docking procedure was employed to uncover crucial details, including the preferred orientation of the anthocyanin molecule relative to the chitosan chain, binding affinity, and underlying molecular interactions between the two components. Initially, the chitin structure was modeled using the Carbohydrate Builder of GlyCam, an online tool specialized in carbohydrate modeling [37]. The resulting chitin structure comprised 16 β -1,4-linked N-acetylglucosamine units saturated with a methyl ester. As illustrated in Figure 3, the acetyl group within the molecular chain of chitin was removed to yield a chitosan structure. The process of deacetylation from chitin to chitosan for molecular dynamics simulations involved using PyMol, a software designed for structural modification and visualization [38], to achieve a complete degree of deacetylation (100%).

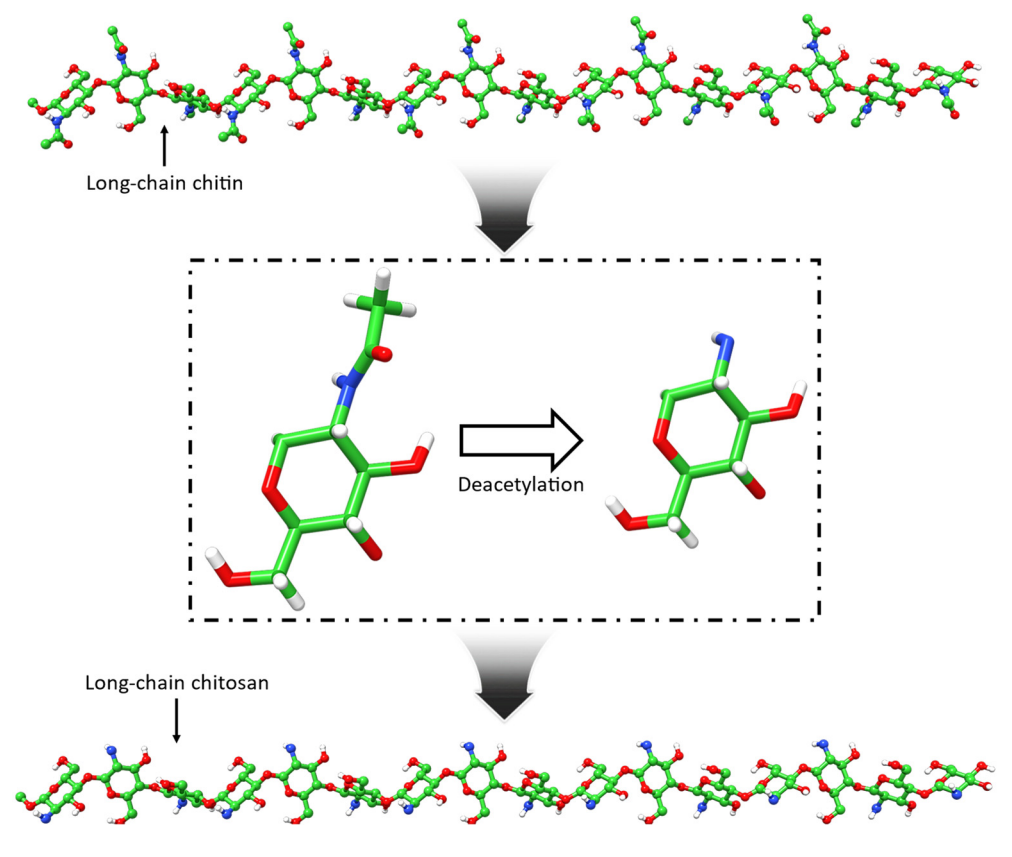


Figure 3. Molecular modeling of chitosan. The modeling of the chitosan structure begins with a long-chain chitin structure model (**top**), followed by the deacetylation process in which N-acetyl groups within the chitin structure are converted into amino (NH₂) groups (**middle**), resulting in a long-chain chitosan structure (**bottom**). The atom representations include green, white, blue, and red for carbon, hydrogen, nitrogen, and oxygen, respectively.

The resulting chitosan structure is shown in Figure 3. Thereafter, additional structural preparations for docking were performed using the dock-prep tool of UCSF Chimera X (version 1.9) [39]. The molecular structure of anthocyanin was obtained from PubChem

Photonics **2025**, 12, 231 9 of 34

(CID: 145858), a repository of chemical compounds. Prior to docking, energy minimization was performed using the conjugate gradient method. The final docking of anthocyanin onto chitosan was conducted using AutoDock software (Vina 1.2.x) for molecular docking and configuration analysis [40]. To complete the analysis, bond analysis, and visualization of the resulting structure were carried out using BIOVIA Discovery Studio Visualizer (version 4.5) [41].

2.8. Determination of Physicochemical Properties

Further assessments were performed to determine the physicochemical properties, including the moisture content, swelling degree, solubility, contact angle, film thickness, water vapor transmission rate, water vapor permeance, and water vapor permeability of the fabricated chitosan film and chitosan-based pH sensor.

2.8.1. Determination of Moisture Content, Swelling Degree, and Solubility

To ascertain the moisture content, swelling degree, and solubility, the films were precisely cut into 2×2 cm² pieces and weighed using an analytical balance (KERN ADB, Analytical balance, KE-ADB200-4-EA, Balingen, Germany) with an accuracy of 0.1 mg, denoted as the initial weight (m₁). The films were then subjected to drying at 60 °C for 6 h to attain the initial dry mass (m₂). Following this, the dried films were immersed in beakers containing 30 mL of distilled water at room temperature (25 °C) for 24 h. The film samples were then extracted from the free water and re-weighed (m₃). Post-immersion, the films underwent another round of drying at 60 °C for 24 h, resulting in the final dry mass (m₄). This entire process was conducted three times for each sample, and the averages were recorded. The following equations were used to compute the characteristics of the films.

$$\%Moisture Content = \frac{m_1 - m_2}{m_1} \times 100$$
 (2)

%Swelling Degree =
$$\frac{m_3 - m_2}{m_2} \times 100$$
 (3)

$$\%Solubility = \frac{m_2 - m_4}{m_2} \times 100 \tag{4}$$

2.8.2. Measurement of Contact Angle and Film Thickness

The contact angles were determined by dispensing 3 μ L of distilled water onto 2 \times 2 cm² film samples using a micropipette. The results are reported as the average of three measurements. The thickness of the films was determined using a digital caliper (CAS Digital Vernier Caliper, DC150-1, Seoul, Republic of Korea). Five random measurements were conducted for each sample, and the resulting thickness was computed as the average of these measurements.

2.8.3. Determination of Water Vapor Transmission Rate, Permeance, and Permeability

To evaluate the water vapor permeability, a wide-mouth cup with a diameter of 5 cm was used. Distilled water (30 mL) was poured into the container, ensuring a headspace of less than 2 cm between the distilled water surface and the sample. The wide-mouth cup was hermetically sealed using a waterproof cover to prevent the water from evaporating along the edges, and the temperature was regulated at 30 $^{\circ}$ C. The system was allowed to stabilize for 3 h to ensure that the water and the cup were at the designated temperature for the experiment. Once the system reached a stable temperature of 30 $^{\circ}$ C, the film was added. The waterproof lid was removed, and the sample was positioned between two gaskets and tightly sealed with a screw lid. It was imperative that the film was correctly aligned, devoid of any cracks or wrinkles, and covered the entire wide opening of the cup. The tests

Photonics **2025**, 12, 231 10 of 34

were conducted at 30 °C for 5 h, providing ample time to attain a dynamic equilibrium of water vapor flux. The data were recorded manually every 20 min.

This method adheres to the ASTM Standard Test Method E96, commonly referred to as the cup method. The weight loss of the cup was measured with a precision of 0.0001 g and plotted as a function of time. The slope was assessed using linear regression. Subsequently, the water vapor transmission rate (WVTR), permeance, and water vapor permeability (WVP) were computed using the following equations:

$$WVTR\left(\frac{g}{s \cdot m^2}\right) = \frac{\Delta w}{\Delta t \cdot A} \tag{5}$$

$$Permeance\left(\frac{g}{s \cdot m^2 \cdot Pa}\right) = \frac{WVTR}{\Delta P}$$
 (6)

$$WVP\left(\frac{g}{s \cdot m \cdot Pa}\right) = Permeance \cdot thickness \tag{7}$$

The flux, denoted as $\Delta w/\Delta t$ (g/s), represents the rate of weight loss of the cell per unit of time. This was determined using the slope of the weight reduction of the cup. The actual exposed area, A (m²), was determined based on the diameter of the mouth cup. At 30 °C, the water vapor pressure differential, ΔP (Pa), was set to 4245 Pa [42], assuming complete water vapor saturation.

2.9. Determination of Mechanical Properties

To examine ultimate tensile strength and elongation at the break of the films, an in-house constructed testing apparatus was utilized. Conforming to the ASTM D882 guidelines, the assessment was conducted with a crosshead speed of 0.02 mm/s and a 10 kg load cell (SMOWO; model RWST01A, Shanghai, China). All measurements were carried out at room temperature. The mechanical properties of each film were evaluated through three distinct measurements, and the data provided encompassed the average values.

2.10. Durability of the Chitosan-Based pH Sensor

To assess the durability of the chitosan-based pH sensors, a stock solution of the extracted anthocyanin was prepared by dissolving the extract in distilled water at a concentration of 0.5 mg/mL. A CCD spectrometer (SM245, wavelength range: 200 nm–1050 nm, optical resolution: 0.3–10 nm FWHM, Kora Spectral Products, Seoul, Republic of Korea) was used to characterize the samples, with a light source covering the UV-Vis range from 357 nm to 900 nm. Test solutions were collected after subjecting the chitosan-based pH sensors to durability tests, where the samples were immersed in water for 0, 30, 60, and 90 min. At each interval, the surrounding water was collected for further analysis. The cuvette path length was maintained at 10 mm for all measurements. All measurements were performed in triplicate to ensure accuracy and reproducibility. In addition, consistent conditions were maintained throughout the experiments.

3. Results and Discussion

3.1. Colorimetric Properties of the Chitosan-Based pH Sensor

The successful extraction of anthocyanins from red cabbage was a pivotal step in developing a chitosan-based pH sensor. Red cabbage anthocyanin exhibits noticeable structural changes, indicating a shift in color with pH variations, spanning from the acidic to the alkaline range. This observed color variation is attributed to the hyperchromic and bathochromic properties inherent in anthocyanins [32,36]. Specifically, anthocyanin transitions to a green or yellow shade in the alkaline region from red or pink in the acidic region, as shown in Figure 4. At extremely low pH, less than 2, the predominant color is

Photonics **2025**, 12, 231 11 of 34

red, resulting from the flavylium cation (Figure 4a). As the pH slightly increases from 2 to 4, a transition toward a purple or blue quinoidal base occurs (Figure 4b,c). Subsequently, under slightly acidic or near-neutral conditions, the color shifts to the dominant colorless carbinol pseudo-base (Figure 4d). A further increase in pH above 7 induces a gradual decline in anthocyanin stability, leading to the formation of a green-yellow color attributed to chalcone formation (Figure 4e) [32]. At higher pH levels, the hydroxide ions (OH⁻) present in the basic environment can accept protons (H⁺) from the anthocyanin molecule. As the pH increases further, this base form can undergo further structural changes, leading to the opening of the central ring in the anthocyanin structure. This ring opening results in the formation of chalcone, which is more stable in basic conditions. This isomerization into chalcone occurs through water-catalyzed tautomerization [43]. Thus, the pigment exists predominantly in its flavylium cation form, which imparts a deep red hue under highly acidic conditions. As the pH increases, the molecule transitions through quinoidal base structures, resulting in a color change from purple to blue. Under alkaline conditions, anthocyanins progressively convert to their chalcone form, leading to green and yellow coloration at higher pH values.

The UV-Vis absorption spectra of red cabbage anthocyanin extracted and analyzed across a pH range of 1 to 13 reveal distinct variations in absorbance intensity and peak positions, which correlate with the structural transformations of the pigment in response to pH changes. The spectra shown in Figure 4f exhibit strong absorption in the visible range, particularly between 520 and 550 nm, corresponding to the flavylium cation, which is the predominant anthocyanin form under highly acidic conditions. As the pH increases, a progressive shift in the absorption maxima is observed due to the stepwise deprotonation of the anthocyanin molecule and the formation of quinoidal bases and other intermediate species. This transition is accompanied by a perceptible color change from red to purple. In the neutral to mildly basic range, a reduction in absorbance intensity is evident, suggesting structural rearrangements and partial degradation of the anthocyanin chromophore.

Under highly alkaline conditions, the absorption spectra exhibit further shifts with diminished intensity, attributed to the formation of the chalcone structure, which results from the opening of the anthocyanin pyran ring under strongly basic conditions. Specifically, from pH 1 to 8, the maximum absorption peak gradually shifts from 524 nm to 537 nm, with a concurrent decrease in absorption intensity as the pH increases. Under highly alkaline conditions (pH > 9), a significant bathochromic shift occurs, with the absorption maximum shifting from 587 nm to 620 nm, indicative of the structural changes associated with anthocyanin degradation and chalcone formation. These spectral variations highlight the sensitivity of red cabbage anthocyanin to pH fluctuations, reinforcing its potential as a natural pH indicator. The observed bathochromic shifts and absorbance changes provide valuable insights into the pigment's stability and its potential applicability in pH-responsive sensing platforms.

The colorimetric response of red cabbage anthocyanins to pH changes has been widely studied, with reports indicating varying sensitivity ranges [44,45]. Our results demonstrate a broad transition from pH 1 to 13, as shown in the UV-Vis spectrum in Figure 4f. This is consistent with the findings of other studies that have observed anthocyanin stability and color variation across a wider pH spectrum. For example, Liu et al. reported color changes from pH 2 to 12 [45], while Vo et al. documented a shift spanning pH 1 to 13 [44]. The extended pH sensitivity observed in our study is due to the full spectrum of structural transformations that anthocyanins undergo in response to protonation or deprotonation. These structural changes, illustrated in Figure 4, explain the observed color variations across the entire pH range. The presence of color changes at extreme pH values, as shown in our results, demonstrates the versatility of red cabbage anthocyanins as a

Photonics **2025**, 12, 231 12 of 34

natural pH indicator with potential applications in food safety, environmental monitoring and biomedical sensing.

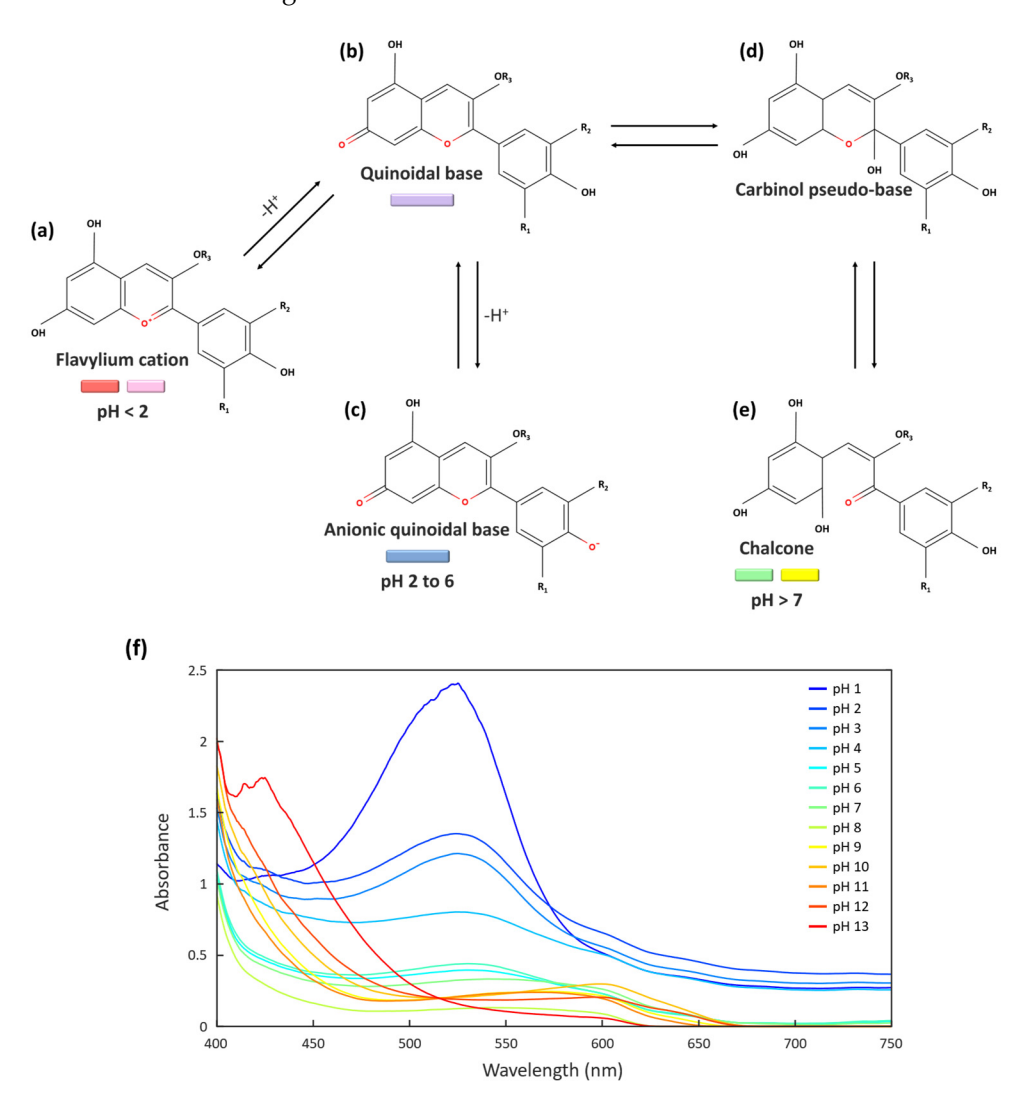


Figure 4. Molecular changes in red cabbage anthocyanin with pH variations. The structural transformations of red cabbage anthocyanin across different pH ranges. The sequence includes changes from (a) flavylium cation (pH: <2) to (b) quinoidal base, (c) anionic quinoidal base, and (d) carbinol pseudo-base (pH: 2–6), and (e) chalcone (pH: >7) structures as pH transitions from acidic to basic regions. (f) UV-Vis absorption spectra from pH 1 to pH 13 of the extracted red cabbage anthocyanin.

As depicted in Figure 5a, the response of the extracted anthocyanin to pH variations was visually evident through the color changes observed in buffer solutions with pH values ranging from 1 to 13. The color of the extracted red cabbage anthocyanin solution undergoes the outlined variations associated with chemical changes when exposed to buffer solutions of varying pH values. Notably, the extracted anthocyanin exhibited a plum color, which transformed to red or pink in acidic solutions and adopted shades of green or yellow in alkaline solutions. The ability of anthocyanin to exhibit distinct colors across a range of pH values makes it valuable for indicating and monitoring pH changes in the surrounding environment. Leveraging these inherent properties, anthocyanin was effectively employed as a pH indicator in the fabrication of a chitosan-based pH sensor.

Photonics **2025**, 12, 231 13 of 34

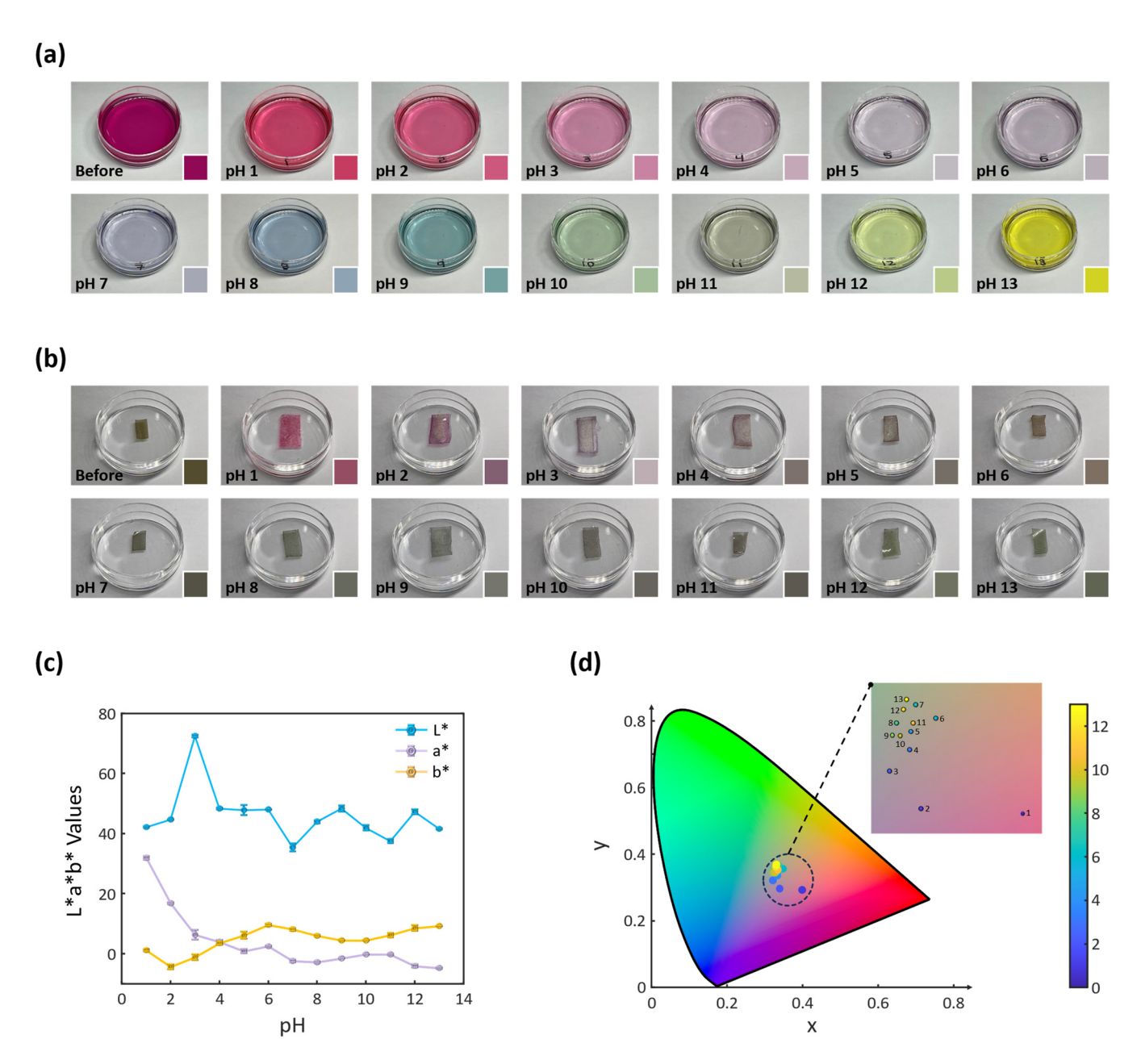


Figure 5. pH-induced color changes in anthocyanin- and chitosan-based pH sensor films. (a) Color transitions of the extracted anthocyanin, starting from its original plum color and changing to red or pink in strongly acidic regions to green or yellow in strongly basic regions when buffer solutions of varying pH are added. (b) Color changes of the fabricated chitosan-based pH sensor films, originally brown, transforming from pink in strongly acidic regions to green in strongly basic regions upon exposure to buffer solutions of different pH values. (c) Plot illustrating the variation in L* a* b* values in response to changing pH levels and (d) visualization of colors associated with specific pH values, plotted on the CIE XYZ color space for chitosan-based pH sensor films.

Figure 5b shows the color changes of the chitosan-based pH sensor when immersed in buffer solutions with pH values ranging from 1 to 13. The sensor demonstrated high sensitivity to pH changes, with rapid and discernible color shifts upon contact with different pH solutions. The observed color variations are attributed to the chemical transformations in the anthocyanin molecules corresponding to the varying pH levels [32,46]. Consequently, the initial brown hue of the chitosan-based pH sensor underwent a color transformation, shifting from pink to purple, then lavender, and finally light gray as the pH increased in the acidic range. Conversely, the sensor retained its original brown color within the

Photonics **2025**, 12, 231 14 of 34

neutral pH region. Notably, as the pH transitioned to the basic range, the sensor exhibited various shades, including dark gray and olive green. These vivid and distinctive color changes highlight the potential applications of the developed films as effective pH sensors across a spectrum of environments, demonstrating their versatility and precision in pH-sensing applications.

In this study, the observed pH domains exhibited distinct color changes at specific pH values and within specific ranges. These domains are categorized as follows: pH 1, pH 2, pH 3, pH 4–6, pH 7, pH 8–10, and pH 11–13, based on the discernible shifts in the slope depicted in Figure 5c. To quantitatively assess the color variations, the L* a* b* model was employed, as illustrated in Figure 5c. Here, the L* value corresponds to brightness, where a positive value indicates a lighter shade and a negative value indicates a darker shade. Additionally, the a* and b* values indicate the position along the red-green and blue-yellow axes, respectively, with positive values signifying a shift toward redness or yellowness and negative values indicating a shift toward greenness or blueness. This comprehensive categorization of pH domains enables a nuanced understanding of how the sensor reacts over a broad range of pH levels. The utilization of the L* a* b* model further provides a quantitative framework for analyzing the colorimetric response of the sensor, enhancing the precision and reliability of pH determinations. This categorization scheme not only indicates the versatility and sensitivity of the sensor but also lays the foundation for its potential applications in various fields necessitating precise pH measurements.

In addition, the various colors associated with the pH values in the CIE XYZ color space depicted in Figure 5d serve as a crucial component for understanding the intricate colorimetric response of the developed pH sensor. The CIE XYZ color space provides a standardized and objective representation of colors, allowing for a systematic analysis of the color change performance across different pH values. Each point in this color space corresponds to a specific color associated with a particular pH, offering a visual mapping of the chromatic transitions of the developed sensor. The dispersion and arrangement of these points also emphasize their ability to distinguish between different pH levels. This vivid representation not only reinforces the versatility of the chitosan-based pH sensor but also highlights its sensitivity to subtle variations in pH-induced color changes. This color space mapping not only validates the efficacy of the sensor but also positions it as a reliable tool for applications demanding accurate and discerning pH measurements, ranging from chemical analysis to biological assays.

Impact of Chitosan Base Color on pH Detection Visibility

The inherent brown hue of the native chitosan, derived from biowaste, posed a significant challenge in the visual detection of pH changes when using the chitosan-based pH sensor. The base color of chitosan interfered with the visibility of the colorimetric shifts induced by the pH-sensitive anthocyanin dye, making the pH changes less discernible to the naked eye. Although color analysis confirmed that the sensor's response to varying pH levels was distinct and did not overlap, the perceptibility of these changes without instrumental assistance was hindered by the chitosan's original coloration. To address this limitation, an additional experiment was conducted involving a bleaching process to enhance the transparency of the chitosan substrate. Specifically, 2.5 g of the as-prepared chitin was added to 150 mL of 6% hydrogen peroxide (H_2O_2) and heated at 60 °C overnight, with continuous stirring at 300 rpm. This bleaching treatment significantly altered the appearance of chitosan, transforming it from its natural brownish color to an almost transparent state, as shown in Figure 6a. Consequently, the chitosan film fabricated from the bleached solution was much lighter in the shade compared to the unbleached variant.

Photonics **2025**, 12, 231 15 of 34

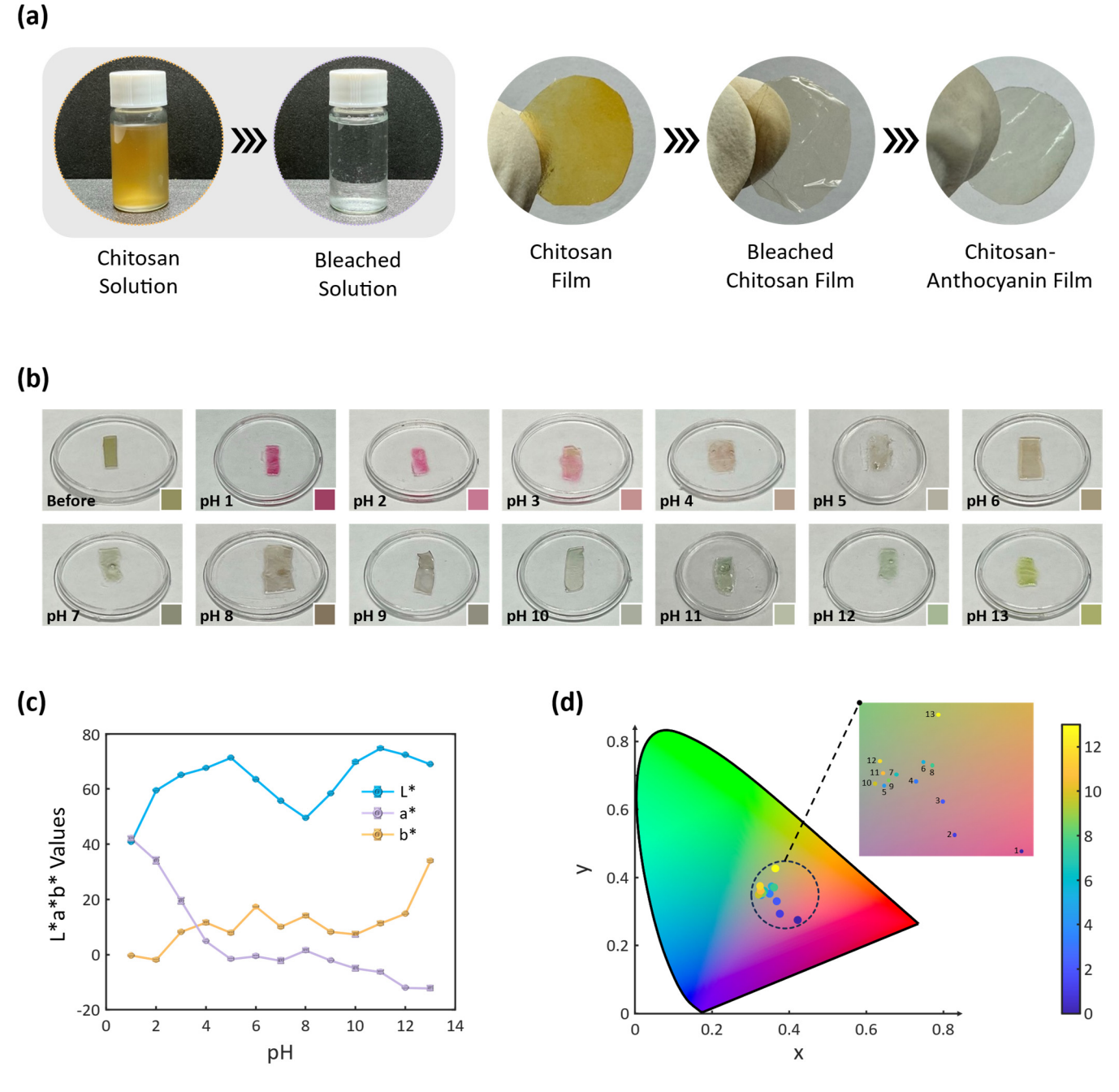


Figure 6. pH-induced color changes in bleached chitosan-based pH sensor films. (a) Comparative images showing the difference between unbleached (brownish) and bleached (nearly transparent) solutions and the resulting films. The bleaching process significantly lightened the chitosan, resulting in a more transparent substrate for the pH sensor. (b) Visual representation of the color changes observed in the bleached chitosan-based pH sensor upon exposure to buffer solutions with pH values ranging from 1 to 13. (c) L* a* b* color space analysis of the bleached sensor, highlighting the clear individual domains corresponding to each pH value. The distinct separation of points illustrates the sensor's enhanced ability to differentiate between pH levels compared to the unbleached sensor. (d) CIE XYZ color space mapping of the sensor's response, showing the distribution of chromatic transitions across different pH levels.

The bleached chitosan substrate, when used to fabricate the pH sensor with anthocyanin, resulted in a sensor with significantly enhanced visual clarity. The subsequent color changes in response to pH variations became significantly more discernible to the naked eye. Figure 6b illustrates the colorimetric response of the sensor fabricated with

Photonics **2025**, 12, 231 16 of 34

bleached chitosan across a pH range of 1 to 13. The sensor exhibited high sensitivity to pH changes, with rapid and distinct color shifts that were easily visible without the need for advanced detection tools. The removal of the base brown color through bleaching not only improved the sensor's visual detectability but also enhanced its user-friendliness, making it more practical for real-world applications where ease of use and rapid interpretation are essential.

Further color analysis was conducted to evaluate the effectiveness of the bleached chitosan-based pH sensor, particularly in terms of the distinctness and discernibility of color changes across different pH levels. The results revealed that the bleached sensor exhibited clear and distinct color domains for each pH value, which were readily perceptible to the naked eye. This improvement is illustrated by the discernible shifts in the slope of the L* a* b* color space model, as depicted in Figure 6c. Unlike the unbleached sensor, which displayed color changes within broader ranges, the bleached sensor demonstrated more precise and well-defined domains, with each individual pH point occupying its own unique space in the colorimetric analysis. This clear separation emphasizes the sensor's enhanced ability to distinguish between different pH levels effectively. Moreover, the performance of the sensor was further validated using the CIE XYZ color space, as shown in Figure 6d. In this analysis, each point within the color space corresponds to a specific color associated with a particular pH value. The visual mapping of chromatic transitions within the bleached chitosan sensor displayed a well-distributed arrangement in the XY plane, further highlighting its superior ability to differentiate between pH values. Although both the bleached and unbleached sensors exhibited no overlapping points in the color space—indicating that each pH value corresponded to a unique color—the bleached sensor exhibited a better distribution of these points, translating into improved visibility and user experience. These vivid and distinctive color changes demonstrate the significant impact of the base color of chitosan on the performance of the fabricated pH sensor. The bleaching process not only enhanced the visual clarity and precision of the colorimetric response but also contributed to a more accurate and reliable pH-sensing capability of the sensor. The improved distribution and separation of color points in the bleached sensor emphasizes its potential for practical applications, where precise and easily interpretable pH monitoring is critical.

The initially fabricated sensors exhibited distinct color changes within defined ranges, which were categorized as pH 1, pH 2, pH 3, pH 4-6, pH 7, pH 8-10, and pH 11-13. These domains were based on discernible shifts in the slope of color analysis. However, to fully capture and highlight these changes, it was essential to address the natural brownish color of the chitosan substrate, which could interfere with the visibility of the colorimetric shifts induced by the pH-sensitive anthocyanin dye. To resolve this, a bleaching procedure was employed to transform the substrate from its natural brownish state to an almost transparent state. As demonstrated, the post-processing step minimized background interference, thereby enhancing the contrast and clarity of the pH-induced colorimetric shifts. A comparison of the results between the natural and bleached states of the chitosan substrate demonstrates the necessity and efficacy of this additional step in ensuring the accuracy and reproducibility of the sensor's performance. The inclusion of the results for both the natural and bleached states also demonstrates the sustainable origin of the chitosan substrate derived from the mealworm biomass. Unlike chitosan derived from other sources, mealworm biomass provides a natural base material with unique properties that can be leveraged to develop eco-friendly and efficient sensors. The natural state of the chitosan substrate offers insight into the raw material's potential, while the bleached state highlights the enhancements achievable through minimal processing.

Photonics **2025**, 12, 231

3.2. Durability, Demonstration, and Sensitivity of the Chitosan-Based pH Sensor

To assess the durability of the chitosan-based pH sensor, the film was immersed in water for 90 min. Figure 7a shows a visual representation of the observed behavior over time. The combination of hydrophobic chitosan and hydrophilic anthocyanins in the developed chitosan-based pH sensor film introduces unique properties that are evident when exposed to water. The durability of the chitosan-based pH sensor was assessed in distilled water to accurately evaluate the potential leaching of anthocyanin without interference from external ions or buffer components. While alternative media such as PBS could have been employed, the presence of salts may interact with the chitosan matrix, potentially affecting the leaching behavior and confounding the assessment of the sensor durability. Using distilled water, we ensured that any observed anthocyanin release was solely attributable to the stability of the sensor, rather than external environmental interactions. This approach provides a clear and controlled evaluation of the sensor's longevity under aqueous conditions.

Anthocyanins, which are water-soluble compounds with an inherent affinity for water molecules, play a pivotal role in the observed changes. Upon exposure to water, the anthocyanins within the film readily absorb water, contributing significantly to the overall swelling of the film. This hydration process is likely to be the primary factor behind the increase in size observed during immersion. In addition, the coexistence of hydrophobic chitosan and hydrophilic anthocyanins introduces a dynamic interplay, leading to non-uniform swelling within the film. The hydrophilic nature of anthocyanins encourages water absorption, creating regions with differential swelling. This uneven swelling can result in the film developing slight folds, as observed after 30 min. The differential swelling phenomenon is a consequence of the distinct water interaction behaviors of chitosan and anthocyanins. Notably, the film retained its color integrity throughout the immersion period in all the solutions. The surrounding water remained visibly clean and devoid of any pigments leached from the film.

Figure 7b further provides a quantitative analysis to assess the potential release of anthocyanin in water based on UV-Vis spectrometry. The results depicted in the absorbance spectra indicate a significant difference between the stock anthocyanin solution and the test solutions obtained from the durability tests of the chitosan-based pH sensors. The stock solution exhibits a pronounced absorbance peak at around 600 nm, reaching a maximum absorbance value of approximately 2. This is consistent with the known optical properties of anthocyanins, which typically display absorbance peaks in the visible region [47], particularly around the red and blue wavelengths, due to their conjugated double-bond structures and chromophore activity. Conversely, the absorbance values for the surrounding water samples collected at 0, 30, 60, and 90 min are substantially lower across the entire wavelength range, suggesting minimal leaching of the anthocyanin from the chitosanbased pH sensors into the surrounding water. The absorbance values remain close to zero, with negligible increases even after 90 min of immersion. This outcome indicates strong durability and retention of the anthocyanin within the chitosan matrix, suggesting that the pH sensors maintain their structural and chemical integrity over the duration of the test. The difference in absorbance between the stock solution and the test samples implies that the anthocyanin was successfully embedded within the chitosan matrix, with minimal dissolution into the water, confirming the effectiveness of the chitosan material as a stable carrier for anthocyanin in aqueous environments. This stability is crucial for the long-term application of these pH sensors, especially in environments where they may be exposed to varying levels of moisture or aqueous media.

This demonstrates the robustness of the developed chitosan-based pH sensor, indicating its color-fastness under prolonged exposure. Understanding the behavior of the

Photonics **2025**, 12, 231 18 of 34

chitosan-based pH sensor in aqueous environments is critical for its application in pH sensing. The ability of the film to undergo controlled changes in size and exhibit folds without compromising its color integrity suggests its potential for dynamic and responsive pH measurements, further validating its suitability for practical pH-sensing applications.

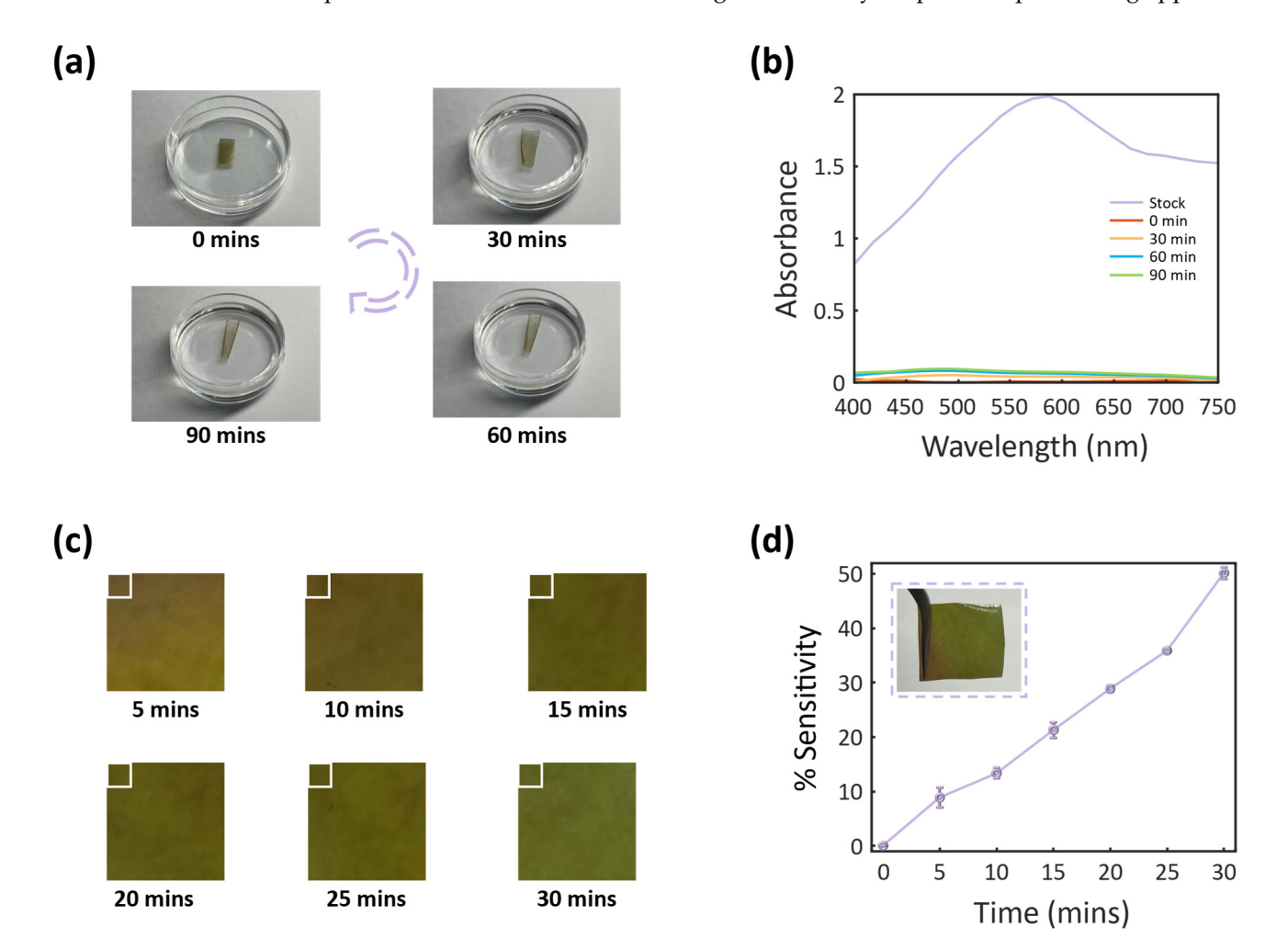


Figure 7. Color-fastness, ammonia assay, and sensitivity of chitosan-based pH sensor films. (a) The chitosan-based pH sensor film was immersed in water for 90 min, and the process was visually depicted at 30 min intervals. This figure captures the observed behavior and changes in the film over time. (b) Assessment of the durability of the chitosan-based pH sensor in water over time. UV-Vis absorption spectra of the extracted anthocyanin (stock) and the surrounding solution after immersing the chitosan-based pH sensor for intervals of 0, 30, 60, and 90 min. (c) Sequential images capturing the color changes of the chitosan-based pH sensor at 5 min intervals for 30 min when exposed to ammonia. The progression from brown to vivid green is visually represented. (d) A plot of the computed sensitivity of the chitosan-based pH sensor over time when exposed to ammonia, providing quantitative insights into the responsiveness of the sensor ammonia with the final film after exposure (insert).

In this study, the color transition of the chitosan-based pH sensor film during the detection of ammonia was visually demonstrated and analyzed. Figure 7c shows a series of images capturing the color changes at different time points after exposure to ammonia with a pH of 11.5, indicating a shift from brown to green. Notably, the color remained consistent after 10 min of exposure and reached an absolute green hue by 30 min. The rapid initial color changes, followed by stabilization at longer times, align with findings from the literature on the response of similar pH sensor films to ammonia gas [48]. This observation is further quantified in Figure 7c, where the sensitivity of the films is plotted against time.

Photonics **2025**, 12, 231 19 of 34

The color sensitivity analysis reveals a progressive change in anthocyanins' color when subjected to ammonia, with a continuous increase over time, reaching a maximum value of 50.16%.

The sensitivity analysis plays a pivotal role in comprehending the reaction of the chitosan-based pH sensor (CPS) to ammonia exposure. As illustrated in Figure 7d, the sensor exhibits a heightened sensitivity over time, suggesting ongoing chemical interactions between the sensor films and ammonia. The ability to detect volatile nitrogen compounds and the observed temporal evolution demonstrate the potential of the CPS for real-time pH monitoring, showcasing its dynamic responsiveness. The ability of the chitosan-based pH sensor films to detect and display color changes in the presence of ammonia also suggests their potential utility in monitoring the freshness of foods. Specifically, one of the most important markers of the quality and freshness of moist foods that are high in protein, including meat and seafood, is the formation of volatile nitrogen molecules. This aligns with previous research that demonstrated color alterations in anthocyanins exposed to ammonia, attributing such changes to underlying modifications in pigment chemistry [48]. Hence, the results of this demonstration highlight the potential use of the developed films, which are based on chitosan and serve as pH sensors to monitor pH changes in real time, thereby showcasing their utility in various practical applications.

3.3. Chemical and Physical Characterization of Chitosan and the Chitosan-Based pH Sensor

The physical, chemical, mechanical, and colorimetric properties, as well as the sensitivity and molecular structure of the fabricated chitosan-based pH sensor films, were explored through systematic analyses and experimentation to probe their efficacy in pH determination. These results offer insights into the nature and capabilities of the developed sensor, opening avenues for its potential use in various fields that require rapid pH measurements.

A comprehensive characterization approach using Fourier-transform infrared (FTIR) spectroscopy was employed to elucidate the chemical properties of the biomass-derived chitosan, anthocyanin extracted from red cabbage, and the resultant chitosan-based pH sensor (CPS). Figure 8 shows the FTIR spectrum of the extracted chitosan, revealing significant bands and peaks that provide detailed insights into its molecular structure and composition. The broadened peak spanning 3410–3150 cm⁻¹ exhibits a robust band, indicating N-H and O-H stretching and intramolecular hydrogen bonding interactions. Absorptive features around 2922 cm⁻¹ and 2877 cm⁻¹ signify symmetric and asymmetric stretching of C-H bonds, characteristic of polysaccharides and consistent with similar spectra of polysaccharide materials like xylan [49] and glucans [50]. Residual N-acetyl groups are evident from bands appearing around 1632 cm⁻¹ (representing C=O stretching of amide I) and 1325 cm⁻¹ (representing C-N stretching of amide III). The spectrum also displays a discernible band at 1546 cm⁻¹, indicative of N-H bending of the primary amine [51]. Notably, the signals at 1456 cm⁻¹ and 1376 cm⁻¹ correspond to CH₂ bending and CH₃ symmetrical deformations, respectively. The absorption band at 1153 cm⁻¹ is attributed to the asymmetric stretching of the C-O-C bridge, while bands at 1064 cm^{-1} and 1013 cm^{-1} correspond to C-O stretching. These observations align with the findings reported by other researchers on FTIR chitosan spectra [52–54].

Considering the extraction of chitosan from mealworm shells, glycosaminoglycan (GAG) contamination could be present. GAGs, a distinct class of polysaccharides, are identifiable by sulfated groups, usually evidenced by robust bands around the 1260–1270 cm⁻¹ region [55]. However, in the chitosan spectrum, a subtle signal at 1261 cm⁻¹ was observed, which was notably faint and insufficient to imply the presence of sulfate groups. This observation effectively dismisses the likelihood of GAG contamination in the chitosan material. The specific signal at 1261 cm⁻¹ is attributed to the bending vibrations of the

Photonics **2025**, 12, 231 20 of 34

hydroxyl groups intrinsic to chitosan [54]. Additionally, the signal at 888 cm $^{-1}$ corresponds to the out-of-plane CH bending of the monosaccharide ring structure [52]. The presence of characteristic functional groups and bonds, as evident from these peaks, indicates the chemical integrity and purity of the fabricated chitosan. The degree of deacetylation (%DD) is a critical parameter for determining the physicochemical properties of chitosan, particularly its solubility, biocompatibility, and film-forming ability. The %DD of the synthesized chitosan was determined using FTIR spectroscopy. The characteristic absorption bands at $1655~\rm cm^{-1}$ (amide I) and $3450~\rm cm^{-1}$ (hydroxyl stretching) were analyzed, and the %DD was calculated based on their intensity ratio following the method outlined by Sánchez-Machado et al. [56]. The resulting %DD was determined to be $97.92 \pm 0.52\%$, indicating a high degree of deacetylation, which enhances chitosan's film-forming capability. This high %DD value contributes to the structural integrity of the sensor, ensuring optimal performance and stability in practical applications.

The FTIR spectra of anthocyanin, shown in Figure 8, reveal distinct characteristic peaks associated with its chemical composition. The peak observed at 1030 cm⁻¹ can be attributed to the stretching vibrations of C-O-C esters, indicating the presence of ester linkages within the molecular structure. The peak at 1089 cm^{-1} is assigned to C-C symmetric stretching, while the peak at 1255 cm^{-1} is indicative of the stretching vibrations of the pyran ring, a common structural feature in flavonoid compounds [57]. Bands in the range of 1300 cm⁻¹ to 1380 cm⁻¹ are associated with C-O angular deformations of phenols, further confirming the presence of phenolic groups. The band at 1405 cm-1 is indicative of the C-O bond. The peaks at 1589 cm⁻¹ and 1701 cm⁻¹ are assigned to the C=C and C=O groups of the aromatic ring, respectively, providing insights into the aromatic nature of the extracted anthocyanin. The presence of peaks at 2848 cm⁻¹ and 2930 cm⁻¹ indicates the asymmetric and symmetric stretching of the C-H bond in the CH₂ group. The broad band in the range of 2985–3590 cm⁻¹ is associated with the O-H group of phenols and sugar vibrations. These identified peaks align well with the reported FTIR spectra of anthocyanin extracts [57–59], affirming the consistency of the obtained results with the expected chemical composition of anthocyanin.

As depicted in Figure 8, the FTIR spectra of the chitosan-based pH sensor (CPS) film exhibit characteristics of both chitosan and anthocyanin. The broadened peak between 3410 cm⁻¹ and 3150 cm⁻¹, which indicates robust N-H and O-H stretching, along with intramolecular hydrogen bonding interactions, demonstrates the presence of chitosan in the CPS. In addition, the absorptive features at 2922 cm⁻¹ and 2877 cm⁻¹ signify the symmetric and asymmetric stretching of C-H bonds. The anthocyanin contribution is evident in the peaks at 1701 cm⁻¹, indicative of C=O groups within the aromatic ring, providing insights into the aromatic nature of the extracted anthocyanin. Furthermore, the contribution of chitosan reveals a discernible band at 1546 cm⁻¹, associated with N-H bending of the primary amine, and additional signals at 1456 cm⁻¹ and 1376 cm⁻¹ corresponding to CH_2 bending and CH_3 symmetrical deformations, respectively. The band at 1325 cm⁻¹ corresponds to the C-N stretching of amide III, indicating the presence of residual N-acetyl groups in the chitosan structure. The peak at $1153 \, \mathrm{cm}^{-1}$ is associated with the asymmetric stretching of the C-O-C bridge, while the absorption bands at 1064 cm⁻¹ and 1013 cm⁻¹ are attributed to the C-O stretching vibrations. These features further confirm the structural integrity of chitosan in the sensor.

In addition, the distinctive peak at 1255 cm⁻¹ in the anthocyanin spectrum corresponds to the stretching vibrations of the pyran ring, a characteristic structural feature of flavonoid compounds. Although both chitosan and anthocyanin bands are evident, the spectrum is predominantly characterized by chitosan bands. Notably, the anthocyanin-associated band at 1701 cm⁻¹ is still visible, indicating the presence of carbonyl groups from the aromatic

Photonics **2025**, 12, 231 21 of 34

structure of anthocyanin. However, more intense bands like those at 1589 cm⁻¹, typically prominent in anthocyanin spectra, may be masked or merged with stronger chitosan peaks due to the overlap in their spectral regions. The anthocyanin bands, while present, are less prominent in comparison, which aligns with the overall composition of the sensor. The coexistence of these characteristic bands from both chitosan and anthocyanin in the chitosan-based pH sensor spectrum, corroborated by their respective FTIR spectra, confirms the successful integration of these components, forming a composite material with a unique molecular fingerprint.

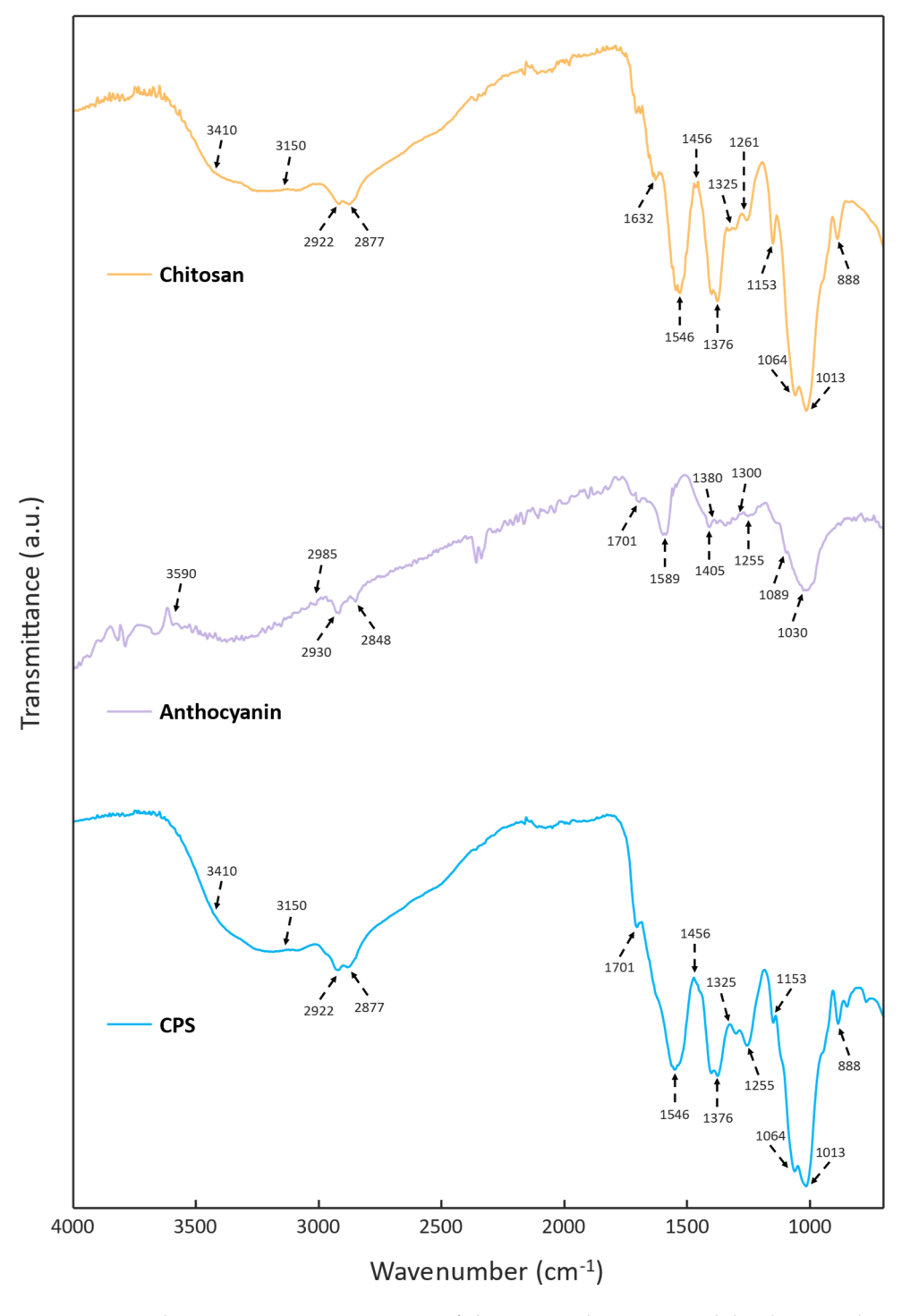


Figure 8. FTIR characterization. FTIR spectra of chitosan, anthocyanin, and the chitosan—based pH sensor (CPS) films, with their respective characteristic peaks indicated.

Photonics **2025**, 12, 231 22 of 34

3.4. Molecular Interaction of Chitosan and Anthocyanin

A molecular docking study between chitosan and anthocyanin was conducted to gain insights into the nature and characteristics of their interactions, shedding light on the potential binding configuration and the stability of the resulting complex. The obtained results, represented by the interaction category, type, distance, and associated angle, as detailed in Table 1, provide a comprehensive overview of the molecular interactions. The conclusive docking configuration illustrated in Figure 9 represents the arrangement with the lowest binding affinity, quantified at -3 kcal/mol. Additionally, the analysis yielded a lower and upper root mean square deviation (RMSD) of 0 Å, indicating that the docked configuration showed no deviation from the reference structure, thereby confirming its stability. The RMSD values serve as metrics to assess the stability and consistency of the docking configuration throughout the simulation, with lower values suggesting a more reliable and tightly bound complex.

Table 1. Analysis of the molecular interactions between chitosan and anthocyanin.

Category	Type	Distance (Å)	Angle
Electrostatic	π -cation	4.14	18.41°
Electrostatic	π -cation	4.29	23.30°
Hydrophobic	π -sigma	2.48	10.68°

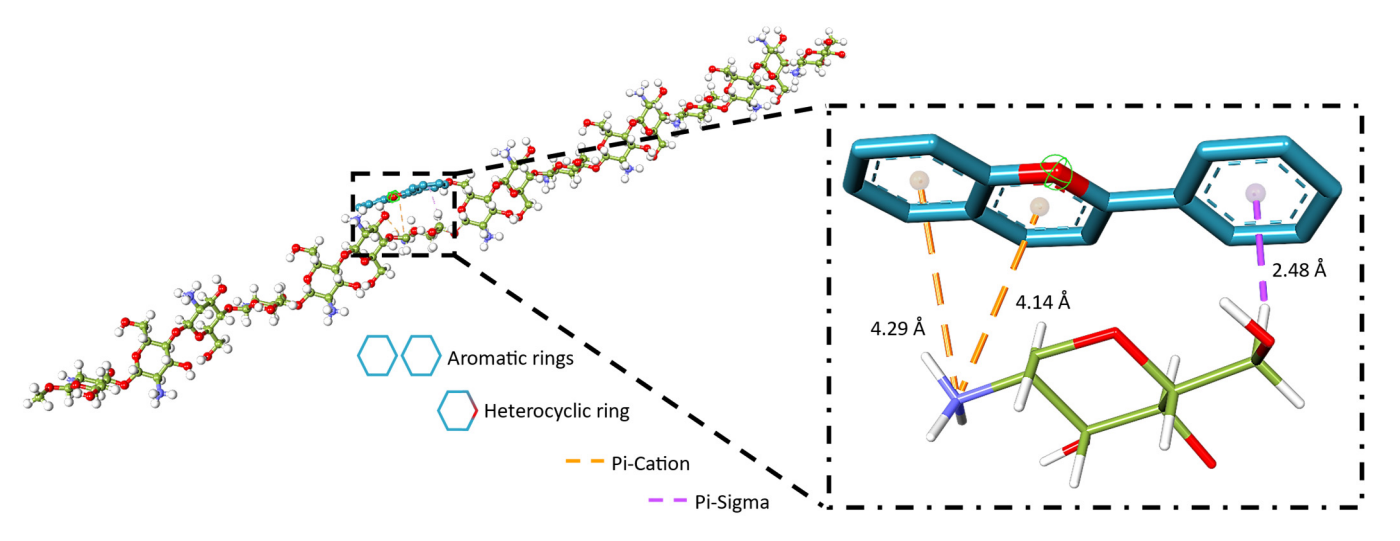


Figure 9. Molecular configuration and interactions between chitosan and anthocyanin. Illustration of molecular interactions between chitosan and anthocyanin. The molecular docking of anthocyanin on the chitosan chain is displayed, highlighting the configuration of the lowest binding affinity and lowest root mean square deviation. The zoomed section provides a detailed view of the intermolecular interactions between chitosan and the rings of anthocyanin. These interactions are categorized as π -cation, representing electrostatic interactions between the protonated amino groups of chitosan and the π -electrons of anthocyanin's aromatic rings, and π -sigma, depicting hydrophobic interactions between the aromatic π -orbitals of anthocyanin and the C-H bonds of chitosan.

As illustrated in Figure 9, two interactions characterized as π -cation demonstrate a consistent pattern of electrostatic interactions between the chains of chitosan and the molecules of anthocyanin. This interaction is marked by an attractive force between the protonated amino groups of chitosan and the π -electrons associated with the aromatic rings of anthocyanin. The process of deacetylation in chitosan results in the generation of multiple free amino groups, enhancing the occurrence of these electrostatic interactions. The specified distance and angle parameters offer precise quantitative insights into the spatial arrangement and strength of the observed electrostatic π -cation interaction. Specifically,

Photonics **2025**, 12, 231 23 of 34

the interaction distance involving the π -orbitals occurs at 4.14 Å with an angle of 18.41°, forming a stable configuration with one of the aromatic rings of anthocyanin. A similar electrostatic π -cation interaction is identified at a slightly extended distance of 4.29 Å, featuring a larger angle of 23.30°. This interaction occurs with the heterocyclic ring (oxygencontaining ring) of the anthocyanin molecule. These observations suggest a recurring theme of electrostatic attraction between the positively charged regions of chitosan and the π -orbitals of anthocyanin. Notably, the electrostatic forces emerge as pivotal contributors to the stabilization of the chitosan-anthocyanin complex. The consistent occurrence of such interactions, characterized by distinct distances and angles, further emphasizes the nature of the electrostatic forces governing the binding between chitosan and anthocyanin.

In addition, a hydrophobic π -sigma interaction was observed. This interaction exists between the aromatic π -orbitals of anthocyanin and C-H bonds of chitosan, occurring at a relatively short distance of 2.48 Å and an angle of 10.68° . Anthocyanins possess both hydrophilic and hydrophobic regions. The hydrophilic components, such as hydroxyl (-OH) groups, facilitate solubility in water. Meanwhile, the hydrophobic nature of the aromatic acyl groups contributes to interactions with nonpolar components, exemplified by the C-H bonds of chitosan. Such non-covalent interactions are prevalent in anthocyanins, where aromatic acyl groups engage in hydrophobic interactions with other molecules [60]. This interaction can shield the chromophoric group from nucleophilic attacks, leading to the formation of a colorless carbinol pseudo-base [60,61].

Hydrophobic forces arise from the intrinsic inclination of nonpolar moieties to minimize their exposure to aqueous environments. Thus, the π -orbitals associated with the aromatic system of anthocyanin form attractive interactions with the C-H bonds of chitosan. The proximity of the participating π -orbitals and C-H bonds plays a decisive role in the observed hydrophobic π -sigma interaction. As these nonpolar components convene at a shorter distance, the resultant complex seeks to minimize its exposure to the surrounding aqueous medium, thereby enhancing the stability of the chitosan-anthocyanin assembly. The consistent presence of electrostatic π -cation interactions, coupled with the distinctive hydrophobic π -sigma interaction, suggests a multi-faceted binding mechanism between chitosan and anthocyanin. The variations in the distances and angles observed in the interactions indicate different binding strengths and orientations, contributing to the overall stability of the chitosan-anthocyanin complex. Therefore, the development of chitosan-based pH sensor films was enabled.

3.5. Physicochemical Properties of Chitosan and the Chitosan-Based pH Sensor

In the pursuit of developing an effective pH sensor, quantifying the moisture content, swelling degree, and solubility is imperative, as these characteristics play a pivotal role in the performance and stability of the sensing material. The fabricated films, comprising pure chitosan (CS) and the developed chitosan-based pH sensor (CPS) incorporating anthocyanin, were analyzed to elucidate their behavior under different conditions. Table 2 summarizes the determined values of these parameters. Notably, their thicknesses were determined to be 0.15 mm and 0.19 mm, respectively. The moisture content of the pure chitosan film was measured at $4.61 \pm 0.02\%$, while that of the chitosan-based pH sensor exhibited a slightly lower moisture content of $4.37 \pm 0.03\%$. The elevated moisture content in the chitosan film is attributed to the intermolecular interactions involving water molecules and hydroxyl/amino groups within the chitosan molecular chains. The introduction of anthocyanin results in robust intermolecular interactions with the amino groups in chitosan chains, consequently restraining water-chitosan interactions and leading to a decreased moisture content. Notably, this aligns with prior findings of decreased moisture content when incorporating an anthocyanin-containing extract into a chitosan matrix [62,63]. The

Photonics **2025**, 12, 231 24 of 34

observed difference emphasizes the role of the pH-sensitive indicator dye—anthocyanin—in modulating moisture absorption, a critical consideration for pH-sensing applications.

Table 2. Thickness, moisture content, swelling degree, and solubility of chitosan and chitosan-based pH sensor films.

Films	Thickness (mm)	Moisture Content (%)	Swelling Degree (%)	Solubility (%)
CS CPS	0.15 ± 0.10 0.19 ± 0.10	$4.61 \pm 0.02 \\ 4.37 \pm 0.03$	$446.33 \pm 0.50 \\ 843.50 \pm 0.60$	$16.24 \pm 0.18 \\ 59.31 \pm 0.20$

The swelling degree, a crucial parameter in pH sensing, was also determined to be 446.33% for the chitosan film and 843.50% for the chitosan-based pH sensor. This substantial disparity is due to the hydrophilic properties of anthocyanin. The increased swelling of the chitosan-based pH sensor is indicative of enhanced water absorption facilitated by the hydrophilic properties of anthocyanin. This characteristic is advantageous for pH sensing, as it implies greater responsiveness to changes in the surrounding environment. The observed swelling behavior aligns with the anticipated influence of the hydrophilic pH-sensitive indicator dye on the responsiveness of the substrate material, thereby contributing to improved pH sensitivity of the sensor. The solubility, which is indicative of the dissolution characteristics of the fabricated films, was 16.24% for the pure chitosan film and 59.84% for the chitosan-based pH sensor. The hydrophobic nature of the chitosan film contributes to its lower solubility, while the introduction of anthocyanin increases solubility due to its hydrophilic nature. The observed increase in solubility aligns with prior research indicating the enhanced water solubility of polymers upon the incorporation of anthocyanins [64,65]. These observed differences demonstrate the potential of the chitosan-based pH sensor for enhanced performance in pH-sensing applications.

Figure 10a shows a droplet of water on the fabricated chitosan film and chitosan-based pH sensor, with a green outline indicating the measured contact angle. The measured contact angles of 111° for pure chitosan and 55° for the chitosan-based pH sensor provide crucial insights into the surface properties of these materials, with significant implications for their performance in pH-sensing applications. The contrast in droplet shapes and contact angles offers a comprehensive view of hydrophobicity, wettability, and adhesion characteristics. The significant disparity in the contact angles suggests a substantial difference in hydrophobicity between pure chitosan and the chitosan-based pH sensor. A contact angle of 111° for pure chitosan indicates a relatively hydrophobic surface, where water beads up, while the reduced contact angle of 55° for the pH sensor implies a more hydrophilic surface. The inclusion of red cabbage anthocyanin, known for its hydrophilic nature and water solubility, contributes to this decrease in contact angle, promoting a surface that is more receptive to water. In addition, the change in the contact angle aligns with the wetting behavior of the films.

A higher contact angle corresponds to poor wetting, indicative of a hydrophobic surface where water beads up, whereas a lower contact angle suggests better wetting and a hydrophilic surface where water spreads out. For pH sensing, a more hydrophilic surface is advantageous because it enhances the interaction with aqueous solutions, leading to improved sensitivity to pH changes. The observed difference in the contact angles also has implications for adhesion. Higher contact angles are often associated with lower adhesion, while lower contact angles suggest better adhesion. The reduced contact angle of the chitosan-based pH sensor may imply enhanced adhesion to the substrate or medium, which is a crucial factor in ensuring the stability and longevity of the sensor in practical applications. These findings highlight the significance of surface properties in tailoring

Photonics **2025**, 12, 231 25 of 34

materials for pH-sensing applications, emphasizing the potential of the chitosan-based pH sensor for enhanced sensitivity and performance.

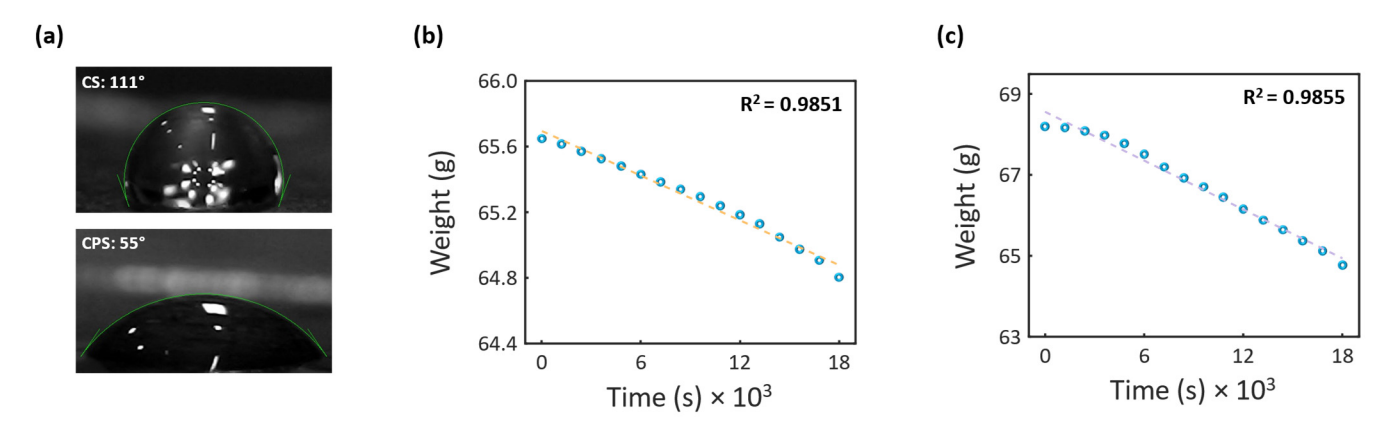


Figure 10. Contact angle and water vapor permeability measurements. (a) Contact angle measurements of the fabricated films: chitosan and chitosan-based pH sensor. Water vapor permeability plot illustrating the relationship between weight loss and time for (b) chitosan and (c) chitosan-based pH sensor films.

The water vapor permeability was further determined for both the chitosan (CS) and the chitosan-based pH sensor (CPS). The analysis of water vapor permeability is instrumental in understanding the permeability characteristics of the fabricated CS and CPS films. The process entails the movement of water molecules to the interface of the film, adsorption at the film surface, dissolution and diffusion within the film matrix, desorption at the other side, and subsequent transportation away from the surface. This phenomenon is influenced by both the inherent morphology of the material, Fick's law of diffusion, and Henry's law of gas solubility, resulting in the observed solubility–diffusion effect. Table 3 summarizes the values obtained from the analysis. The WVP values obtained for the CS and CPS films were 1.93×10^{-10} g/(m·Pa·s) and 3.83×10^{-10} g/(m·Pa·s), respectively. The water vapor transmission rate (WVTR) for CS was 0.0009 g/(m²·s), while for CPS, it was 0.0040 g/(m²·s). Additionally, the water vapor permeances of CS and CPS were 2.13×10^{-7} and 9.50×10^{-7} g/(m²·Pa·s), respectively. The R-squared values for both films were high—98.51% and 98.55%—emphasizing the linear nature of the mass loss with time, as shown in Figure 10b,c. This indicates a strong correlation between the reduction in mass and elapsed time during the water vapor permeability analysis. The notable difference in water vapor permeability between the chitosan and chitosan-based pH sensor films can be attributed to the introduction of hydrophilic anthocyanin into the chitosan polymer matrix. This facilitates greater water vapor absorption and transmission through the film. Hence, the higher hydrophilicity of the CPS film results in an increased affinity for water vapor in CPS compared to CS, leading to the observed higher WVTR and WVP values.

Table 3. Water vapor permeability (WVP), water vapor permeance, and water vapor transmission rate (WVTR) of chitosan and chitosan-based pH sensor films.

Films	WVP	Permeance	WVTR	R-Squared
	(g/smPa)	(g/sm ² Pa)	(g/sm²)	(%)
CS CPS	1.93×10^{-10} 3.83×10^{-10}	$2.13 \times 10^{-7} $ 9.50×10^{-7}	0.0009 0.0040	98.51 98.55

The high permeability of the CPS film is favorable for several reasons, including rapid response, increased sensitivity, and improved adhesion. Firstly, enhanced permeability

Photonics **2025**, 12, 231 26 of 34

facilitates a more responsive interaction between the sensor film and its surrounding environment, allowing for quicker and more efficient detection of changes in pH. This is particularly crucial in applications where rapid and real-time tracking of pH variations is essential, such as assessing freshness in the food industry or conducting medical diagnostics. Moreover, higher permeability can contribute to improved sensitivity and accuracy of pH measurements. A film with increased permeability is more receptive to the ingress of ions or molecules associated with pH changes, leading to a more pronounced and easily detectable response. This heightened sensitivity is advantageous for ensuring that the CPS can effectively capture subtle alterations in the environment, providing precise and reliable data. Additionally, in applications where the CPS needs to be in direct contact with a substrate or medium, a higher permeability can enhance adhesion. Improved adhesion ensures better contact between the sensor and the surface, promoting stability and longevity in practical applications. This is particularly important under various environmental conditions, which necessitate a strong and stable connection for consistent and accurate pH monitoring.

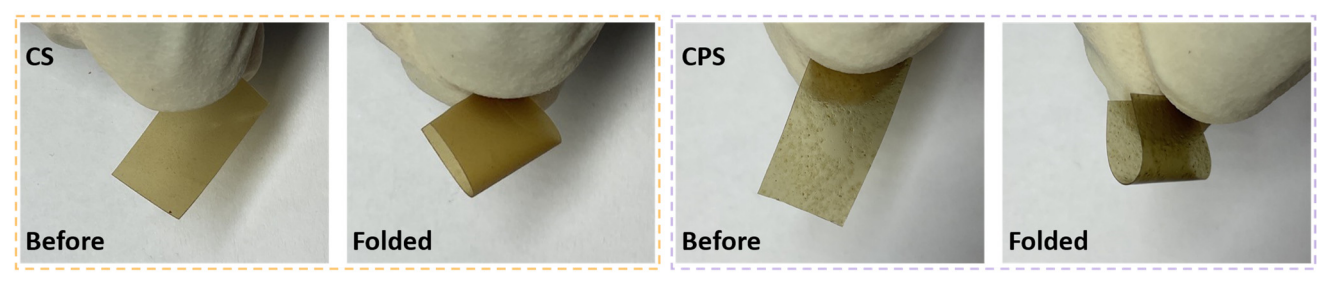
3.6. Mechanical Properties of Chitosan and the Chitosan-Based pH Sensor

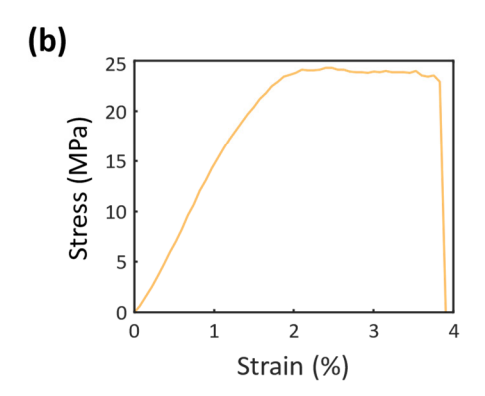
The flexibility of films is a crucial aspect in various applications, including sensor technologies. Figure 11a shows a visual representation of the flexibility of pure chitosan and the chitosan-based pH sensor. Both films were evaluated for their flexibility by examining their response to folding, and the results offer insights into their mechanical properties. As shown in Figure 11a, both the pure chitosan film and the chitosan-based pH sensor are shown in their flat (undeformed) and deformed (folded) states. The purpose of this demonstration was to show the flexibility of the films and specifically to highlight that the addition of anthocyanin does not compromise the inherent flexibility of the chitosan-based pH sensor. In comparison, it is evident that both maintain a degree of flexibility, even when subjected to folding. The pure chitosan film exhibits an inherent flexibility that allows it to deform when subjected to external forces, while the chitosan-based pH sensor, due to the addition of anthocyanin, demonstrates improved flexibility. This observation is noteworthy as it indicates that the incorporation of anthocyanin into the pH sensor formulation does not hinder or diminish the observed flexibility. In addition, the consistent flexibility observed in both films suggests a cohesive and well-blended composition, affirming the successful integration of anthocyanin without compromising the mechanical properties.

Furthermore, the mechanical characteristics of chitosan-based pH sensor (CPS) films significantly influence their efficacy as sensors. The stress-strain plots illustrated in Figure 11b,c demonstrate the response of the chitosan film and the CPS to uniaxial tensile load, allowing a thorough examination of their mechanical behavior by assessing crucial parameters such as ultimate tensile strength (UTS) and elongation at break (EAB). The UTS and EAB serve as indicators of the material's mechanical rigidity and flexibility, respectively. In the tensile test, the chitosan film exhibited UTS and EAB values of 24 MPa and 3.9%, respectively, whereas the CPS exhibited UTS and EAB values of 8.8 MPa and 8.4%, respectively. The decrease in the ultimate tensile strength of CPS can be attributed to the plasticizing impact of anthocyanin within the chitosan matrix, leading to enhanced molecular mobility [66]. Despite the reduction in tensile strength, the addition of anthocyanin significantly increased the EAB, indicating improved flexibility—an essential characteristic for pH-sensing applications. The ability of the CPS to undergo deformation without losing flexibility is crucial for its adaptability to different surfaces and environments. Thus, the flexibility of CPS ensures that it can conform to varying shapes and contours, which is a desirable feature in sensor applications where adaptability to different substrates is often required.

Photonics **2025**, 12, 231 27 of 34

(a)





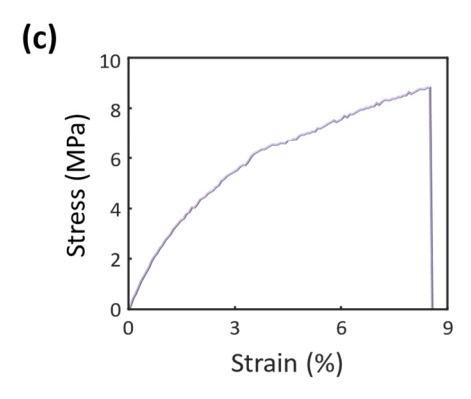


Figure 11. Mechanical properties of chitosan-based pH sensor films. (a) Visual representation demonstrating the flexibility of both the chitosan and chitosan-based pH sensor films. The stress-strain curves elucidate the mechanical properties of (b) chitosan and (c) chitosan-based pH sensors.

After the incorporation of anthocyanin into the chitosan matrix, the resulting composite material was further characterized to ensure that the fundamental physical, chemical, and mechanical properties of the chitosan substrate were not degraded. This step was critical for validating the substrate's integrity and confirming that the observed colorimetric responses were due solely to the interaction of anthocyanin with varying pH levels rather than changes in the chitosan matrix itself. FTIR analysis provided evidence of the successful integration of anthocyanin within the chitosan matrix, as indicated by the appearance of anthocyanin-specific functional group peaks. This also confirmed the compatibility of the dye with the chitosan substrate and ensured its uniform distribution, which is essential for the sensor's reproducibility and consistent performance. By performing this re-characterization, we demonstrate that the incorporation of anthocyanin does not compromise the substrate's structural integrity, thus supporting the reliability of the developed sensor across diverse pH-sensitive applications.

3.7. Comparison of the Chitosan-Based pH Sensor to Existing Colorimetric pH Sensors

Chitosan derived from mealworm shells represents a sustainable approach by utilizing biowaste, reducing environmental impact, and promoting circular economy practices. Other natural sources of biomass for chitosan extraction include crustacean shells (e.g., shrimp and crab shells) and fungal cell walls. Compared to these sources, mealworm-derived chitosan offers unique advantages such as faster production cycles, a lower environmental footprint, and reduced reliance on marine ecosystems. Additionally, the mealworm shells used in this study were produced in a controlled smart farming system, ensuring consistent quality. Recent studies have extensively explored the integration of red cabbage anthocyanin into chitosan-based systems for pH-responsive sensing, particularly in food packaging applications. Chen et al. [67] successfully immobilized anthocyanins into chitosan/oxidized chitin nanocrystal composites, demonstrating distinct color changes

Photonics 2025, 12, 231 28 of 34

in response to ammonia vapor and acidic/alkaline conditions. Their smart films effectively monitored seafood freshness by detecting ammonia released during spoilage, a principle that aligns with our demonstration of ammonia detection using our sensor. Similarly, Park et al. [68] developed chitosan-based edible films incorporating red cabbage anthocyanins as spoilage indicators, further validating the practical applications of anthocyanin-based sensors for food monitoring. Vo et al. [44] synthesized pH-indicative films by blending chitosan and poly(vinyl alcohol), which showed a sequential color transition as the pork belly underwent spoilage.

The optical properties of anthocyanin-based sensors are primarily governed by the pigment's halochromic behavior, which leads to distinct color variations in response to pH changes. Our study builds upon these findings by extending the measurable pH range from 1 to 13, significantly expanding the potential applications of anthocyanin-based sensors beyond food monitoring to include biomedical diagnostics and environmental sensing. By providing a detailed analysis of the structural transformations of anthocyanin under varying pH conditions, we offer mechanistic insights into its colorimetric behavior, enhancing the understanding of its stability and responsiveness in different environments. A key innovation in our approach is the utilization of chitosan derived from mealworm shells, an underutilized biowaste material, as a sensor substrate. Unlike conventional sources of chitosan, such as shrimp and crab shells, which require extensive processing and contribute to marine waste, mealworm-derived chitosan presents a more sustainable alternative. Mealworms are widely cultivated as a protein source, generating significant quantities of chitin-rich exoskeletons as byproducts of their cultivation. Repurposing these byproducts not only reduces waste but also promotes a circular economy by transforming agricultural residues into high-value, functional materials.

This sustainable fabrication approach minimizes reliance on synthetic polymers and reduces the environmental impact associated with chemical processing. By leveraging biowaste for sensor development, our work aligns with the growing emphasis on green technology and resource efficiency. Furthermore, the eco-friendly nature of the chitosan matrix enhances the sensor's biocompatibility, making it suitable for applications in biomedical fields such as wound monitoring and non-invasive diagnostic tools. In environmental monitoring, the sensor's ability to detect pH fluctuations across a wide range presents opportunities for water quality assessment and pollution detection. By integrating biowaste valorization with advanced sensor technology, this study demonstrates a practical and scalable strategy for developing sustainable materials while addressing critical challenges in healthcare and environmental protection. These advancements not only demonstrate the potential of sustainable materials and eco-friendly processes in sensor development but also establish a framework for future studies exploring the integration of biomaterials into functional devices.

Table 4 presents a comparison of the physical properties of red cabbage anthocyanin-based pH sensors using various substrates, including tensile strength, elongation at break, and water solubility of the substrates. In comparison to other pH sensors that incorporate red cabbage anthocyanin, the chitosan-based film developed in this study demonstrates significant advantages in terms of sustainability, eco-friendliness, and physical characteristics. The sensor, fabricated from biomass-derived chitosan, exhibits a comparable increase in water solubility and water vapor permeability (WVP) to other natural substrates, such as bacterial cellulose membranes and konjac glucomannan. These increases in solubility are attributable to the biodegradable nature of the materials. However, the observed decrease in tensile strength in the chitosan-based film mirrors the trends observed in other natural films, such as those made from corn starch and polyvinyl alcohol nanofibers, where moisture absorption reduces material rigidity. Despite this reduction in tensile strength, the chitosan

Photonics 2025, 12, 231 29 of 34

film demonstrates improved elongation at break, indicating that it can endure greater deformation before failure. This property is similarly noted in bacterial cellulose nanofibers and chitosan/oxidized chitin nanocrystal films. This flexibility is essential for applications requiring mechanical durability, particularly under variable environmental conditions. Furthermore, while substrates such as cationic guar gum films and poly(ethylene glycol) diacrylate show minimal changes in moisture adsorption, the slight increase in the water solubility of the chitosan-based film does not compromise its structural integrity, as confirmed by durability tests (Figure 7). The fabricated chitosan-based pH sensor is distinct because of its use of biomass, contributing to environmental sustainability by repurposing materials that would otherwise be discarded as waste. This film provides an optimal combination of mechanical flexibility, water solubility, and durability, making it a promising alternative to synthetic and other natural pH sensors for various applications.

Table 4. Comparison of substrate materials for colorimetric pH sensing using red cabbage anthocyanin.

Substrate	Form	Physical Properties	Tensile Strength	Elongation at Break	References
Bacterial cellulose membrane	Film	Increase in water solubility	Decrease	Increase	[65]
Corn starch	Film	Increase in thickness and water solubility	No significant change	No significant change	[64]
Bacterial cellulose nanofibers	Nanofiber mat	Increase in moisture absorption	Decrease	Increase	[69]
Chitosan/oxidized chitin nanocrystals	Film	Decrease in WVP	Decrease	Increase	[67]
Cationic guar gum/hydroxyethyl cellulose	Film	Decrease in WVP	Increase (≤3%) Decrease (5%)	Increase (≤3%) Decrease (5%)	[70]
Polyvinyl alcohol	Nanofiber mat	Increase in moisture adsorption	Decrease	Increase	[71]
Poly (ethylene glycol) diacry- late/lignocellulose nanofiber	Hydrogel	No significant change in moisture adsorption	-	-	[72]
Konjac glucoman- nan/oxidized chitin nanocrystals	Film	Increase in water solubility and WVP	Decrease	Decrease	[73]
Biomass-derived Chitosan	Film	Increase in water solubility and WVP	Decrease	Increase	Present work

4. Conclusions

In conclusion, our study has successfully developed a bio pH sensor using chitosan extracted from biomass and incorporating anthocyanin derived from red cabbage. The chitosan-based pH sensor exhibited remarkable proficiency in detecting a broad spectrum of pH levels, as evidenced by a distinctive color shift from pink to green, providing a clear visual indication of pH changes. The low contact angle observed in the sensor suggests enhanced adhesion, which is a pivotal factor for stability and longevity in practical applications. Furthermore, our investigation into the response of the chitosan-based pH sensor to ammonia demonstrated its ability to detect volatile nitrogen compounds, showcasing its potential application in monitoring the freshness of moist, protein-rich foods. Additionally, the color sensitivity analysis indicated a progressive color change in anthocyanins upon exposure to ammonia.

Photonics 2025, 12, 231 30 of 34

The maintained flexibility of the sensor is essential for its integration into pH sensor technologies, allowing adaptation to various surfaces and environments, and highlighting its versatility. Notably, our findings indicate remarkable durability and sustained color stability over extended periods, affirming the suitability of the chitosan-based pH sensor for practical applications. Its inherent biocompatibility and flexibility demonstrate its adaptability, presenting numerous promising applications. The potential of the chitosan-based pH sensor for real-time and continuous pH monitoring and diagnostic applications, and its versatility for a wide range of uses make it a promising candidate for future research and development. Future work will focus on addressing the variability in the extract composition and enhancing the accuracy of our measurements. This will involve further optimization of the fabrication technique by conducting more comprehensive batch comparisons and developing more robust calibration techniques. We will explore the sensor's durability in ionic environments, such as buffered and saline solutions, to assess potential interactions with external ions. Additionally, strategies like cross-linking or polymer blending may be considered to further enhance sensor stability. We will also explore the application of our sensor for monitoring spoilage across a variety of food products. Additionally, we plan to investigate the use of different natural dye sources to further expand the sensor's applicability and performance in various pH-sensitive environments.

Furthermore, we will employ computational methods to study the interactions between chitosan and these dyes in diverse chemical environments to gain a deeper understanding of their compatibility and stability. We also plan to integrate machine learning algorithms to analyze and predict variations in extract quality and incorporate IoT to enable real-time monitoring and data collection. These advancements aim to significantly improve the precision and reliability of our sensor technology, thereby broadening its applicability and effectiveness across various fields. By harnessing chitosan derived from biomass waste and anthocyanin extracted from red cabbage, this research provides an economically feasible and environmentally sustainable strategy for pH sensing. The approach utilized not only contributes to ecological responsibility but also propels the development of sustainable colorimetric pH-sensing methods, addressing environmental concerns and fostering sustainable sensing technologies.

Author Contributions: Conceptualization, E.E.N.-O., R.M., S.-H.H., D.Y. and A.A.; Data curation, E.E.N.-O., R.M., S.-H.H., D.Y., A.A. and C.S.M.; Formal analysis, E.E.N.-O., R.M., S.-H.H., D.Y., A.A. and C.S.M.; Funding acquisition, S.H.C.; Investigation, E.E.N.-O., R.M., S.-H.H., D.Y. and A.A.; Methodology, E.E.N.-O., R.M., S.-H.H., D.Y., A.A. and C.S.M.; Project administration, S.H.C.; Resources, H.-W.J., S.-W.K., Y.-S.S. and S.H.C.; Supervision, A.A., H.-W.J., S.-W.K., Y.-S.S. and S.H.C.; Validation, E.E.N.-O., R.M., S.-H.H., D.Y., A.A., C.S.M., H.-W.J., S.-W.K., Y.-S.S. and S.H.C.; Visualization, E.E.N.-O., R.M., S.-H.H., D.Y. and A.A.; Writing—original draft, E.E.N.-O., R.M., S.-H.H., D.Y. and A.A.; Writing—review and editing, E.E.N.-O., R.M., S.-H.H., D.Y., A.A., H.-W.J., S.-W.K., Y.-S.S. and S.H.C. All authors have read and agreed to the published version of the manuscript.

Funding: This work was carried out with the support of the "Research Program for Agriculture Science & Technology Development (Project No. RS-2024-00399478)" Rural Development Administration, Republic of Korea. This work was supported by the National Research Foundation of Korea (NRF), a grant funded by the Korean government (MSIT) (No. 2022R1C1C1011328).

Institutional Review Board Statement: Not applicable.

Informed Consent Statement: Not applicable.

Data Availability Statement: The data presented in this study are available from the corresponding authors upon request.

Conflicts of Interest: The authors declare no conflicts of interest.

Photonics **2025**, 12, 231 31 of 34

References

1. Baranwal, J.; Barse, B.; Gatto, G.; Broncova, G.; Kumar, A. Electrochemical sensors and their applications: A review. *Chemosensors* **2022**, *10*, 363. [CrossRef]

- 2. He, Q.; Wang, B.; Liang, J.; Liu, J.; Liang, B.; Li, G.; Long, Y.; Zhang, G.; Liu, H. Research on the construction of portable electrochemical sensors for environmental compounds quality monitoring. *Mater. Today Adv.* **2023**, *17*, 100340. [CrossRef]
- 3. Jiang, W.; Lee, S.; Zan, G.; Zhao, K.; Park, C. Alternating Current Electroluminescence for Human-Interactive Sensing Displays. *Adv. Mater.* **2024**, *36*, 2304053. [CrossRef] [PubMed]
- 4. Li, L.; Chen, J.; Xiao, C.; Luo, Y.; Zhong, N.; Xie, Q.; Chang, H.; Zhong, D.; Xu, Y.; Zhao, M. Recent advances in photoelectrochemical sensors for detection of ions in water. *Chin. Chem. Lett.* **2023**, *34*, 107904. [CrossRef]
- 5. Mazur, F.; Han, Z.; Tjandra, A.D.; Chandrawati, R. Digitalization of Colorimetric Sensor Technologies for Food Safety. *Adv. Mater.* **2024**, *36*, e2404274. [CrossRef] [PubMed]
- 6. Ha, J.-H.; Jeong, Y.; Ahn, J.; Hwang, S.; Jeon, S.; Kim, D.; Ko, J.; Kang, B.; Jung, Y.; Choi, J. A wearable colorimetric sweat pH sensor-based smart textile for health state diagnosis. *Mater. Horiz.* **2023**, *10*, 4163–4171. [CrossRef]
- 7. Unger, K.; Greco, F.; Coclite, A.M. Temporary Tattoo pH Sensor with pH-Responsive Hydrogel via Initiated Chemical Vapor Deposition. *Adv. Mater. Technol.* **2022**, *7*, 2100717. [CrossRef]
- 8. Anastasova, S.; Crewther, B.; Bembnowicz, P.; Curto, V.; Ip, H.M.; Rosa, B.; Yang, G.-Z. A wearable multisensing patch for continuous sweat monitoring. *Biosens. Bioelectron.* **2017**, *93*, 139–145. [CrossRef]
- 9. Wang, L.; Wang, J.; Fan, C.; Xu, T.; Zhang, X. Skin-like hydrogel-elastomer based electrochemical device for comfortable wearable biofluid monitoring. *Chem. Eng. J.* **2023**, 455, 140609. [CrossRef]
- 10. Mariani, F.; Serafini, M.; Gualandi, I.; Arcangeli, D.; Decataldo, F.; Possanzini, L.; Tessarolo, M.; Tonelli, D.; Fraboni, B.; Scavetta, E. Advanced wound dressing for real-time pH monitoring. *ACS Sens.* **2021**, *6*, 2366–2377. [CrossRef]
- 11. Parlak, M.E.; Sahin, O.I.; Dundar, A.N.; Saricaoglu, F.T.; Smaoui, S.; Goksen, G.; Koirala, P.; Al-Asmari, F.; Nirmal, N.P. Natural colorant incorporated biopolymers-based pH-sensing films for indicating the food product quality and safety. *Food Chem.* **2024**, 439, 138160. [CrossRef] [PubMed]
- 12. Huang, W.; Wang, X.; Xia, J.; Li, Y.; Zhang, L.; Feng, H.; Zhang, X. Flexible sensing enabled agri-food cold chain quality control: A review of mechanism analysis, emerging applications, and system integration. *Trends Food Sci. Technol.* **2023**, *133*, 189–204. [CrossRef]
- 13. Shen, J.; Xiao, Q.; Sun, P.; Feng, J.; Xin, X.; Yu, Y.; Qi, W. Self-assembled chiral phosphorescent microflowers from Au nanoclusters with dual-mode pH sensing and information encryption. *ACS Nano* **2021**, *15*, 4947–4955. [CrossRef] [PubMed]
- 14. Ma, J.; Jiao, Z.; Zhao, M.; Kong, X.; Xie, H.; Zhang, Z. A fluorescence probe for monitoring toxic hypochlorous acid in biosystems and environmental waters with a broad pH adaptation. *Ecotoxicol. Environ. Saf.* **2024**, 288, 117370. [CrossRef]
- 15. Ding, H.; Tan, P.; Fu, S.; Tian, X.; Zhang, H.; Ma, X.; Gu, Z.; Luo, K. Preparation and application of pH-responsive drug delivery systems. *J. Control. Release* **2022**, *348*, 206–238. [CrossRef]
- 16. Islam, S. Fast responsive anatase nanoparticles coated fiber optic pH sensor. J. Alloys Compd. 2021, 850, 156246. [CrossRef]
- 17. Safitri, E.; Humaira, H.; Murniana, M.; Nazaruddin, N.; Iqhrammullah, M.; Md Sani, N.D.; Esmaeili, C.; Susilawati, S.; Mahathir, M.; Latansa Nazaruddin, S. Optical pH Sensor based on immobilization anthocyanin from Dioscorea alata L. onto polyelectrolyte complex pectin–chitosan membrane for a determination method of salivary pH. *Polymers* 2021, 13, 1276. [CrossRef]
- 18. Promphet, N.; Rattanawaleedirojn, P.; Siralertmukul, K.; Soatthiyanon, N.; Potiyaraj, P.; Thanawattano, C.; Hinestroza, J.P.; Rodthongkum, N. Non-invasive textile based colorimetric sensor for the simultaneous detection of sweat pH and lactate. *Talanta* **2019**, 192, 424–430. [CrossRef]
- 19. Yapor, J.P.; Alharby, A.; Gentry-Weeks, C.; Reynolds, M.M.; Alam, A.M.; Li, Y.V. Polydiacetylene nanofiber composites as a colorimetric sensor responding to Escherichia coli and pH. *ACS Omega* **2017**, 2, 7334–7342. [CrossRef]
- 20. Finnegan, M.; Duffy, E.; Morrin, A. The determination of skin surface pH via the skin volatile emission using wearable colorimetric sensors. *Sens. Bio-Sens. Res.* **2022**, *35*, 100473. [CrossRef]
- 21. Heckmann, L.-H.; Andersen, J.L.; Gianotten, N.; Calis, M.; Fischer, C.H.; Calis, H. Sustainable mealworm production for feed and food. In *Edible Insects in Sustainable Food Systems*; Springer: Cham, Switzerland, 2018; pp. 321–328.
- 22. Aranaz, I.; Alcántara, A.R.; Civera, M.C.; Arias, C.; Elorza, B.; Heras Caballero, A.; Acosta, N. Chitosan: An overview of its properties and applications. *Polymers* **2021**, *13*, 3256. [CrossRef]
- 23. Bhatt, P.; Joshi, S.; Bayram, G.M.U.; Khati, P.; Simsek, H. Developments and application of chitosan-based adsorbents for wastewater treatments. *Environ. Res.* **2023**, 226, 115530. [CrossRef]
- Keshvardoostchokami, M.; Majidi, M.; Zamani, A.; Liu, B. A review on the use of chitosan and chitosan derivatives as the bioadsorbents for the water treatment: Removal of nitrogen-containing pollutants. *Carbohydr. Polym.* 2021, 273, 118625. [CrossRef] [PubMed]
- 25. Manna, S.; Seth, A.; Gupta, P.; Nandi, G.; Dutta, R.; Jana, S.; Jana, S. Chitosan derivatives as carriers for drug delivery and biomedical applications. *ACS Biomater. Sci. Eng.* **2023**, *9*, 2181–2202. [CrossRef]

Photonics **2025**, 12, 231 32 of 34

26. Haider, A.; Khan, S.; Iqbal, D.N.; Khan, S.U.; Haider, S.; Mohammad, K.; Mustfa, G.; Rizwan, M.; Haider, A. Chitosan as a tool for tissue engineering and rehabilitation: Recent developments and future perspectives—A review. *Int. J. Biol. Macromol.* **2024**, 278, 134172. [CrossRef]

- 27. Seino, H.; Kawaguchi, N.; Arai, Y.; Ozawa, N.; Hamada, K.; Nagao, N. Investigation of partially myristoylated carboxymethyl chitosan, an amphoteric-amphiphilic chitosan derivative, as a new material for cosmetic and dermal application. *J. Cosmet. Dermatol.* 2021, 20, 2332–2340. [CrossRef] [PubMed]
- 28. Aouadi, A.; Hamada Saud, D.; Rebiai, A.; Achouri, A.; Benabdesselam, S.; Mohamed Abd El-Mordy, F.; Pohl, P.; Ahmad, S.F.; Attia, S.M.; Abulkhair, H.S. Introducing the antibacterial and photocatalytic degradation potentials of biosynthesized chitosan, chitosan–ZnO, and chitosan–ZnO/PVP nanoparticles. *Sci. Rep.* **2024**, *14*, 14753. [CrossRef]
- 29. Rosales, T.K.O.; Fabi, J.P. Nanoencapsulated anthocyanin as a functional ingredient: Technological application and future perspectives. *Colloids Surf. B Biointerfaces* **2022**, 218, 112707. [CrossRef] [PubMed]
- 30. Cai, D.; Li, X.; Chen, J.; Jiang, X.; Ma, X.; Sun, J.; Tian, L.; Vidyarthi, S.K.; Xu, J.; Pan, Z. A comprehensive review on innovative and advanced stabilization approaches of anthocyanin by modifying structure and controlling environmental factors. *Food Chem.* **2022**, *366*, 130611. [CrossRef]
- 31. Gençdağ, E.; Özdemir, E.E.; Demirci, K.; Görgüç, A.; Yılmaz, F.M. Copigmentation and stabilization of anthocyanins using organic molecules and encapsulation techniques. *Curr. Plant Biol.* **2022**, *29*, 100238. [CrossRef]
- 32. Abedi-Firoozjah, R.; Yousefi, S.; Heydari, M.; Seyedfatehi, F.; Jafarzadeh, S.; Mohammadi, R.; Rouhi, M.; Garavand, F. Application of red cabbage anthocyanins as pH-sensitive pigments in smart food packaging and sensors. *Polymers* **2022**, *14*, 1629. [CrossRef] [PubMed]
- 33. Islam, N.; Hoque, M.; Taharat, S.F. Recent advances in extraction of chitin and chitosan. *World J. Microbiol. Biotechnol.* **2023**, *39*, 28. [CrossRef] [PubMed]
- 34. Mohan, K.; Ganesan, A.R.; Ezhilarasi, P.; Kondamareddy, K.K.; Rajan, D.K.; Sathishkumar, P.; Rajarajeswaran, J.; Conterno, L. Green and eco-friendly approaches for the extraction of chitin and chitosan: A review. *Carbohydr. Polym.* **2022**, 287, 119349. [CrossRef]
- 35. Mwita, C.S.; Muhammad, R.; Nettey-Oppong, E.E.; Enkhbayar, D.; Ali, A.; Ahn, J.; Kim, S.-W.; Seok, Y.-S.; Choi, S.H. Chitosan Extracted from the Biomass of Tenebrio molitor Larvae as a Sustainable Packaging Film. *Materials* **2024**, *17*, 3670. [CrossRef] [PubMed]
- 36. Ghareaghajlou, N.; Hallaj-Nezhadi, S.; Ghasempour, Z. Red cabbage anthocyanins: Stability, extraction, biological activities and applications in food systems. *Food Chem.* **2021**, *365*, 130482. [CrossRef]
- 37. GLYCAM Web. Complex Carbohydrate Research Center, University of Georgia, Athens, GA, USA. Available online: http://glycam.org (accessed on 17 June 2024).
- 38. Schrödinger, L.a.W.D. PyMOL. Available online: http://www.pymol.org/pymol (accessed on 17 June 2024).
- 39. Pettersen, E.F.; Goddard, T.D.; Huang, C.C.; Couch, G.S.; Greenblatt, D.M.; Meng, E.C.; Ferrin, T.E. UCSF Chimera—a visualization system for exploratory research and analysis. *J. Comput. Chem.* **2004**, *25*, 1605–1612. [CrossRef]
- 40. Trott, O.; Olson, A.J. AutoDock Vina: Improving the speed and accuracy of docking with a new scoring function, efficient optimization, and multithreading. *J. Comput. Chem.* **2010**, *31*, 455–461. [CrossRef]
- 41. Discovery Studio. Accelrys [2.1]. Available online: https://www.3ds.com/products/biovia/discovery-studio (accessed on 30 June 2024).
- 42. Cazón, P.; Morales-Sanchez, E.; Velazquez, G.; Vázquez, M. Measurement of the water vapor permeability of chitosan films: A laboratory experiment on food packaging materials. *J. Chem. Educ.* **2022**, *99*, 2403–2408. [CrossRef]
- 43. Saptarini, N.M.; Suryasaputra, D.; Nurmalia, H. Application of Butterfly Pea (Clitoria ternatea Linn) extract as an indicator of acid-base titration. *J. Chem. Pharm. Res.* **2015**, *7*, 275–280.
- 44. Vo, T.-V.; Dang, T.-H.; Chen, B.-H. Synthesis of intelligent pH indicative films from chitosan/poly (vinyl alcohol)/anthocyanin extracted from red cabbage. *Polymers* **2019**, *11*, 1088. [CrossRef]
- 45. Liu, D.; Cui, Z.; Shang, M.; Zhong, Y. A colorimetric film based on polyvinyl alcohol/sodium carboxymethyl cellulose incorporated with red cabbage anthocyanin for monitoring pork freshness. *Food Packag. Shelf Life* **2021**, *28*, 100641. [CrossRef]
- 46. Williams, M.; Hrazdina, G. Anthocyanins as food colorants: Effect of pH on the formation of anthocyanin-rutin complexes. *J. Food Sci.* **1979**, *44*, 66–68. [CrossRef]
- 47. Pratiwi, D.D.; Nurosyid, F.; Supriyanto, A.; Suryana, R. Optical properties of natural dyes on the dye-sensitized solar cells (DSSC) performance. *J. Phys. Conf. Ser.* **2016**, *776*, 012007. [CrossRef]
- 48. Tavassoli, M.; Alizadeh Sani, M.; Khezerlou, A.; Ehsani, A.; Jahed-Khaniki, G.; McClements, D.J. Smart biopolymer-based nanocomposite materials containing pH-sensing colorimetric indicators for food freshness monitoring. *Molecules* **2022**, 27, 3168. [CrossRef]

Photonics **2025**, 12, 231 33 of 34

49. Melo-Silveira, R.F.; Fidelis, G.P.; Costa, M.S.S.P.; Telles, C.B.S.; Dantas-Santos, N.; de Oliveira Elias, S.; Ribeiro, V.B.; Barth, A.L.; Macedo, A.J.; Leite, E.L. In vitro antioxidant, anticoagulant and antimicrobial activity and in inhibition of cancer cell proliferation by xylan extracted from corn cobs. *Int. J. Mol. Sci.* 2011, 13, 409–426. [CrossRef] [PubMed]

- 50. Wolkers, W.F.; Oliver, A.E.; Tablin, F.; Crowe, J.H. A Fourier-transform infrared spectroscopy study of sugar glasses. *Carbohydr. Res.* **2004**, 339, 1077–1085. [CrossRef]
- 51. Lim, S.-H.; Hudson, S.M. Synthesis and antimicrobial activity of a water-soluble chitosan derivative with a fiber-reactive group. *Carbohydr. Res.* **2004**, 339, 313–319. [CrossRef]
- 52. Queiroz, M.F.; Teodosio Melo, K.R.; Sabry, D.A.; Sassaki, G.L.; Rocha, H.A.O. Does the use of chitosan contribute to oxalate kidney stone formation? *Mar. Drugs* **2014**, *13*, 141–158. [CrossRef]
- 53. Vino, A.B.; Ramasamy, P.; Shanmugam, V.; Shanmugam, A. Extraction, characterization and in vitro antioxidative potential of chitosan and sulfated chitosan from Cuttlebone of Sepia aculeata Orbigny, 1848. *Asian Pac. J. Trop. Biomed.* **2012**, 2, S334–S341. [CrossRef]
- 54. Song, C.; Yu, H.; Zhang, M.; Yang, Y.; Zhang, G. Physicochemical properties and antioxidant activity of chitosan from the blowfly Chrysomya megacephala larvae. *Int. J. Biol. Macromol.* **2013**, *60*, 347–354. [CrossRef]
- 55. Costa, M.S.S.P.; Costa, L.S.; Cordeiro, S.L.; Almeida-Lima, J.; Dantas-Santos, N.; Magalhães, K.D.; Sabry, D.A.; Albuquerque, I.R.L.; Pereira, M.R.; Leite, E.L. Evaluating the possible anticoagulant and antioxidant effects of sulfated polysaccharides from the tropical green alga Caulerpa cupressoides var. flabellata. *J. Appl. Phycol.* 2012, 24, 1159–1167. [CrossRef]
- 56. Sánchez-Machado, D.I.; López-Cervantes, J.; Escárcega-Galaz, A.A.; Campas-Baypoli, O.N.; Martínez-Ibarra, D.M.; Rascón-León, S. Measurement of the degree of deacetylation in chitosan films by FTIR, 1H NMR and UV spectrophotometry. Methods X 2024, 12, 102583. [CrossRef] [PubMed]
- 57. Pereira, V.A.; de Arruda, I.N.Q.; Stefani, R. Active chitosan/PVA films with anthocyanins from Brassica oleraceae (Red Cabbage) as Time–Temperature Indicators for application in intelligent food packaging. *Food Hydrocoll.* **2015**, *43*, 180–188. [CrossRef]
- 58. Homayoonfal, M.; Mousavi, M.; Kiani, H.; Askari, G.; Desobry, S.; Arab-Tehrany, E. Modifying the stability and surface characteristic of anthocyanin compounds incorporated in the nanoliposome by chitosan biopolymer. *Pharmaceutics* **2022**, *14*, 1622. [CrossRef] [PubMed]
- 59. Csóka, L.; Dudić, D.; Petronijević, I.; Rozsa, C.; Halasz, K.; Djoković, V. Photo-induced changes and contact relaxation of the surface AC-conductivity of the paper prepared from poly(ethyleneimine)–TiO₂–anthocyanin modified cellulose fibers. *Cellulose* **2015**, 22, 779–788. [CrossRef]
- 60. Wang, J.; Zhao, Y.; Sun, B.; Yang, Y.; Wang, S.; Feng, Z.; Li, J. The structure of anthocyanins and the copigmentation by common micromolecular copigments: A review. *Food Res. Int.* **2024**, *176*, 113837. [CrossRef]
- 61. Matsufuji, H.; Kido, H.; Misawa, H.; Yaguchi, J.; Otsuki, T.; Chino, M.; Takeda, M.; Yamagata, K. Stability to light, heat, and hydrogen peroxide at different pH values and DPPH radical scavenging activity of acylated anthocyanins from red radish extract. *J. Agric. Food Chem.* 2007, 55, 3692–3701. [CrossRef]
- 62. Yong, H.; Wang, X.; Bai, R.; Miao, Z.; Zhang, X.; Liu, J. Development of antioxidant and intelligent pH-sensing packaging films by incorporating purple-fleshed sweet potato extract into chitosan matrix. *Food Hydrocoll.* **2019**, *90*, 216–224. [CrossRef]
- 63. Wang, X.; Yong, H.; Gao, L.; Li, L.; Jin, M.; Liu, J. Preparation and characterization of antioxidant and pH-sensitive films based on chitosan and black soybean seed coat extract. *Food Hydrocoll.* **2019**, *89*, 56–66. [CrossRef]
- 64. Prietto, L.; Mirapalhete, T.C.; Pinto, V.Z.; Hoffmann, J.F.; Vanier, N.L.; Lim, L.-T.; Dias, A.R.G.; da Rosa Zavareze, E. pH-sensitive films containing anthocyanins extracted from black bean seed coat and red cabbage. *Lwt* 2017, 80, 492–500. [CrossRef]
- 65. Kuswandi, B.; Asih, N.P.; Pratoko, D.K.; Kristiningrum, N.; Moradi, M. Edible pH sensor based on immobilized red cabbage anthocyanins into bacterial cellulose membrane for intelligent food packaging. *Packag. Technol. Sci.* 2020, 33, 321–332. [CrossRef]
- 66. Liang, T.; Sun, G.; Cao, L.; Li, J.; Wang, L. A pH and NH3 sensing intelligent film based on Artemisia sphaerocephala Krasch. gum and red cabbage anthocyanins anchored by carboxymethyl cellulose sodium added as a host complex. *Food Hydrocoll.* **2019**, 87, 858–868. [CrossRef]
- 67. Chen, M.; Yan, T.; Huang, J.; Zhou, Y.; Hu, Y. Fabrication of halochromic smart films by immobilizing red cabbage anthocyanins into chitosan/oxidized-chitin nanocrystals composites for real-time hairtail and shrimp freshness monitoring. *Int. J. Biol. Macromol.* 2021, 179, 90–100. [CrossRef] [PubMed]
- 68. Park, K.J.; Lee, J.-S.; Jo, H.J.; Kim, E.S.; Lee, H.G. Antimicrobial and indicator properties of edible film containing clove bud oil-loaded chitosan capsules and red cabbage for fish preservation. *Int. J. Biol. Macromol.* **2022**, *196*, 163–171. [CrossRef]
- 69. Pourjavaher, S.; Almasi, H.; Meshkini, S.; Pirsa, S.; Parandi, E. Development of a colorimetric pH indicator based on bacterial cellulose nanofibers and red cabbage (*Brassica oleraceae*) extract. *Carbohydr. Polym.* **2017**, *156*, 193–201. [CrossRef]
- Chu, M.; Feng, N.; An, H.; You, G.; Mo, C.; Zhong, H.; Pan, L.; Hu, D. Design and validation of antibacterial and pH response of
 cationic guar gum film by combining hydroxyethyl cellulose and red cabbage pigment. *Int. J. Biol. Macromol.* 2020, 162, 1311–1322.
 [CrossRef]

Photonics **2025**, 12, 231 34 of 34

71. Maftoonazad, N.; Ramaswamy, H. Design and testing of an electrospun nanofiber mat as a pH biosensor and monitor the pH associated quality in fresh date fruit (Rutab). *Polym. Test.* **2019**, *75*, 76–84. [CrossRef]

- 72. Safitri, E.A.; Mahendra, I.P.; Putra, A.E.; Ghifari, M.A.; Yanti, D.D.; Yusnaidar, Y.; Ariwahjoedi, B.; Mendez, J.A. Multicolor PEGDA/LCNF hydrogel in the presence of red cabbage anthocyanin extract. *Gels* **2021**, *7*, 160. [CrossRef]
- 73. Wu, C.; Li, Y.; Sun, J.; Lu, Y.; Tong, C.; Wang, L.; Yan, Z.; Pang, J. Novel konjac glucomannan films with oxidized chitin nanocrystals immobilized red cabbage anthocyanins for intelligent food packaging. *Food Hydrocoll.* **2020**, *98*, 105245. [CrossRef]

Disclaimer/Publisher's Note: The statements, opinions and data contained in all publications are solely those of the individual author(s) and contributor(s) and not of MDPI and/or the editor(s). MDPI and/or the editor(s) disclaim responsibility for any injury to people or property resulting from any ideas, methods, instructions or products referred to in the content.